

AD-A055 520

CONSTRUCTION ENGINEERING RESEARCH LAB (ARMY) CHAMPAI--ETC F/G 11/6
FRACTURE CHARACTERISTICS OF ASTM A-607 PIPE-LINE STEEL, ASTM A---ETC(U)
MAY 78 J K SCOTT

UNCLASSIFIED

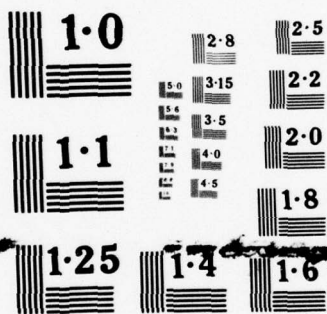
CERL-TR-M-238

NL

| OF |
ADA
055520



END
DATE
FILMED
8-78
DDC



NATIONAL BUREAU OF STANDARDS
MICROCOPY RESOLUTION TEST CHART

FOR FURTHER TRAN

construction
engineering
research
laboratory

TECHNICAL REPORT M-238
May 1978

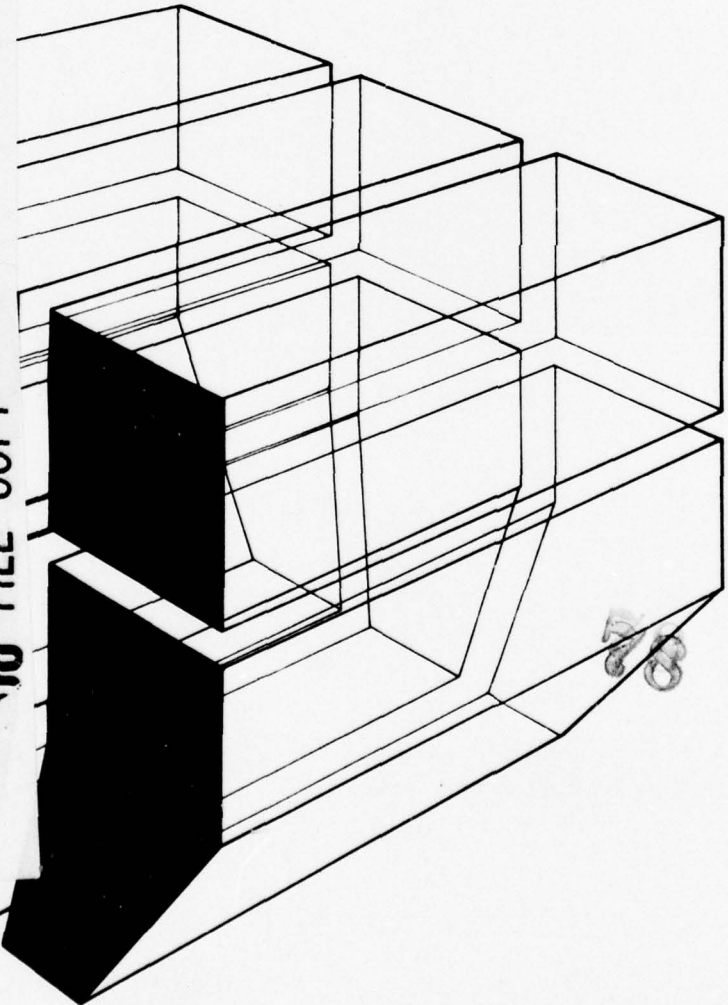
FRACTURE CHARACTERISTICS OF ASTM A-607
PIPELINE STEEL, ASTM A-516 STRUCTURAL STEEL,
AND ASTM B-209, ALUMINUM ALLOYS 5083 AND 6061

12
B-5

AD A 055520

by
J. K. Scott

AD No. —
DDC FILE COPY



DDC
RECEIVED
JUN 23 1978
B

78
06-08 014



The contents of this report are not to be used for advertising, publication, or promotional purposes. Citation of trade names does not constitute an official indorsement or approval of the use of such commercial products. The findings of this report are not to be construed as an official Department of the Army position, unless so designated by other authorized documents.

***DESTROY THIS REPORT WHEN IT IS NO LONGER NEEDED
DO NOT RETURN IT TO THE ORIGINATOR***

UNCLASSIFIED

SECURITY CLASSIFICATION OF THIS PAGE (When Data Entered)

REPORT DOCUMENTATION PAGE		READ INSTRUCTIONS BEFORE COMPLETING FORM
1. REPORT NUMBER CERL-TR-M-238	2. GOVT ACCESSION NO.	3. RECIPIENT'S CATALOG NUMBER
4. TITLE (and Subtitle) FRACTURE CHARACTERISTICS OF ASTM A-607 PIPE- LINE STEEL, ASTM A-516 STRUCTURAL STEEL, AND ASTM B-209, ALUMINUM ALLOYS 5083 and 6061		5. TYPE OF REPORT & PERIOD COVERED FINAL rept.
7. AUTHOR(s) J. K./Scott		6. PERFORMING ORG. REPORT NUMBER
9. PERFORMING ORGANIZATION NAME AND ADDRESS CONSTRUCTION ENGINEERING RESEARCH LABORATORY P.O. Box 4005 Champaign, IL 61820		8. CONTRACT OR GRANT NUMBER(s)
11. CONTROLLING OFFICE NAME AND ADDRESS		10. PROGRAM ELEMENT, PROJECT, TASK AREA & WORK UNIT NUMBERS 4A761102AT23-A2-002
14. MONITORING AGENCY NAME & ADDRESS (if different from Controlling Office)		12. REPORT DATE May 1978
		13. NUMBER OF PAGES 45
		15. SECURITY CLASS. (of this report) Unclassified
16. DISTRIBUTION STATEMENT (of this Report) Approved for public release; distribution unlimited.		15a. DECLASSIFICATION/DOWNGRADING SCHEDULE
17. DISTRIBUTION STATEMENT (of the abstract entered in Block 20, if different from Report)		
18. SUPPLEMENTARY NOTES Copies are obtainable from National Technical Information Service Springfield, VA 22151		
19. KEY WORDS (Continue on reverse side if necessary and identify by block number) fracture characteristics hydrogen embrittlement fatigue striae		
20. ABSTRACT (Continue on reverse side if necessary and identify by block number) The fracture characteristics of two steels (ASTM A-516 and A-607) and two alumi- niums (ASTM B-209, alloys 5083 and 6061) were analyzed under tensile, fatigue, and impact loading conditions. The effect of hydrogen embrittlement on the steels' behavior when fractured under tensile and fatigue conditions was investigated.		

DD FORM 1 JAN 73 1473

EDITION OF 1 NOV 65 IS OBSOLETE

UNCLASSIFIED

SECURITY CLASSIFICATION OF THIS PAGE (When Data Entered)

UNCLASSIFIED

SECURITY CLASSIFICATION OF THIS PAGE(When Data Entered)

Block 20 continued.

The steels were found to be somewhat susceptible to hydrogen embrittlement, with the ASTM A-607 being more susceptible than the ASTM A-516.

The aluminums produced very ductile failures and well-defined fatigue striae.

UNCLASSIFIED

SECURITY CLASSIFICATION OF THIS PAGE(When Data Entered)

FOREWORD

This investigation was conducted by the Engineering and Materials Division of the U. S. Army Construction Engineering Research Laboratory (CERL). The study was sponsored by the Directorate of Military Construction, Office of the Chief of Engineers (OCE), under Project 4A761102AT23, "Structural Systems"; Scientific Area A2; "Facility Components"; and Work Unit 002, "Characterization of Fracture of Engineering Materials." The QCDO Number for this project is 2.02.001.

The OCE technical monitor is I. A. Schwartz.

CERL personnel connected with the investigation were J. Scott, E. Cox, and R. Hannan. Dr. G. R. Williamson is Chief of the Engineering and Materials Division.

COL J. E. Hays is Commander and Director of CERL, and Dr. L. R. Shaffer is Technical Director.

ACCESSION		
NFC	INDEX Section	<input checked="" type="checkbox"/>
DOC	FILE Section	<input type="checkbox"/>
SPATIAL		<input type="checkbox"/>
AUTHORITY		
BY		
DISTRIBUTION/AVAILABILITY CODES		
Dist.	AVAIL	and/or SPECIAL
A		

78 06 08 014

CONTENTS

DD FORM 1473	1
FOREWORD	3
LIST OF TABLES AND FIGURES	5
1 INTRODUCTION	9
Objective	
Approach	
Mode of Technology Transfer	
Background	
2 EXPERIMENTAL PROCEDURE	11
Material	
Specimen Fabrication and Testing	
Hydrogen Embrittlement	
3 RESULTS AND DISCUSSION	12
ASTM A-516 Steel	
ASTM A-607 Steel	
ASTM B-209, Aluminum Alloy 5083	
ASTM B-209, Aluminum Alloy 6061	
4 CONCLUSIONS	14
REFERENCES	14
FIGURES	16
DISTRIBUTION	

TABLES

Number	Page
1 Chemical Composition of Materials	11
2 Mechanical Properties of Steels and Aluminums	11
3 Absorbed Impact Energies of Materials	12

FIGURES

Number	Page
1 Typical Equiaxed Dimple Structure Containing Inclusions, 4250X	16
2 Typical Elongated Dimple Structure, 3750X	16
3 Typical Cleavage Facets, 400X	17
4 Typical Fatigue Striations, 4000X	17
5 Microstructure of ASTM A-516 Steel, 320X	18
6 Microstructure of ASTM A-607 Steel	18
7 Microstructure of ASTM B-209, Al Alloy 5083	19
8 Microstructure of ASTM B-209, Al Alloy 6061	19
9 Specimen Geometry for Tensile, Fatigue, and Charpy Impact Tests	20
10 Tensile Fracture Surface of A-516 Steel, 12X	21
11 Dimple Rupture in A-516 Steel, 1200X	21
12 Fatigue Fracture Surface of A-516 Steel, 8X	22
13 Dimple Rupture in an A-516 Fatigue Specimen, 1000X	22
14 Transgranular Fracture in an A-516 Fatigue Specimen, 650X	23
15 Tensile Fracture Surface of Hydrogen-Embrittled A-516 Steel, 11X	23
16 Fatigue Fracture Surface of Hydrogen-Embrittled A-516 Steel, 12X	24
17 Dimple Rupture in a Hydrogen-Embrittled A-516 Steel, 800X	24

FIGURES (cont'd)

Number	Page
18 Fatigue Striations in A-516 Steel, 1800X	25
19 Fracture Surface of an A-516 Charpy Specimen Tested at -196°C, 11X	25
20 Cleavage Facets in an A-516 Charpy Specimen Tested at -196°C, 550X	26
21 A-516 Steel Charpy Impact Specimen Tested at 0°C, 11X	26
22 A-516 Steel Charpy Impact Specimen Tested at 25°C, 11X	27
23 A-516 Steel Charpy Impact Specimen Tested at 100°C, 11X	27
24 Tensile Fracture Surface of A-607 Steel, 11X	28
25 Dimple Rupture in A-607 Steel, 800X	28
26 Fatigue Fracture Surface of A-607 Steel, 12X	29
27 Fatigue Striations in A-607 Steel, 1000X	29
28 Hydrogen-Embrittled Tensile A-607 Steel Specimen, 11X	30
29 Hydrogen-Embrittled Fatigue A-607 Steel Specimen, 12X	30
30 Fatigue Striae in a Hydrogen-Embrittled A-607 Steel Specimen, 1000X	31
31 A-607 Charpy Impact Specimen Tested at -196°C, 11X	31
32 Cleavage Facets in an A-607 Charpy Impact Specimen Tested at -196°C, 550X	32
33 A-607 Charpy Impact Specimen Tested at 0°C, 9X	32
34 Dimple Rupture in an A-607 Charpy Impact Specimen Tested at 0°C, 300X	33
35 A-607 Charpy Impact Specimen Tested at 25°C, 10X	33
36 Dimple Rupture in an A-607 Charpy Impact Specimen Tested at 25°C, 250X	34

FIGURES (cont'd)

Number	Page
37 A-607 Charpy Impact Specimen Tested at 100°C, 10X	34
38 Dimple Rupture and a Large Inclusion in an A-607 Charpy Impact Specimen Tested at 100°C, 500X	35
39 Tensile Fracture Surface of a 5083 Aluminum Specimen, 9X	35
40 Dimple Rupture in 5083 Aluminum, 450X	36
41 Fracture Surface of 5083 Aluminum Tensile Specimen, 12X	36
42 Dimple Rupture in 5083 Aluminum, 300X	37
43 Fatigue Striae in 5083 Aluminum, 300X	37
44 Fatigue Striae in 5083 Aluminum, 1000X	38
45 5083 Aluminum Charpy Impact Specimen Tested at -196°C, 10X	38
46 5083 Aluminum Charpy Impact Specimen Tested at 0°C, 11X	39
47 5083 Aluminum Charpy Impact Specimen Tested at 25°C, 11X	39
48 5083 Aluminum Charpy Impact Specimen Tested at 100°C, 11X	40
49 Tensile Fracture Surface of 6061 Aluminum, 10X	40
50 Dimple Rupture in 6061 Aluminum Fracture Surface, 300X	41
51 Fatigue Fracture Surface of 6061 Aluminum, 13X	41
52 Dimple Rupture in 6061 Aluminum Fatigue Fracture Surface, 300X	42
53 Fatigue Striae in 6061 Aluminum, 300X	42
54 6061 Aluminum Charpy Impact Specimen Tested at -196°C, 11X	43
55 Dimple Rupture in 6061 Aluminum Charpy Impact Specimen Tested at -196°C, 550X	43

FIGURES (cont'd)

Number		Page
56	6061 Aluminum Charpy Impact Specimen Tested at 0°C, 10X	44
57	6061 Aluminum Charpy Impact Specimen Tested at 25°C, 11X	44
58	6061 Aluminum Charpy Impact Specimen Tested at 100°C, 11X	45

FRACTURE CHARACTERISTICS OF ASTM A-607 PIPELINE STEEL, ASTM A-516 STRUCTURAL STEEL, AND ASTM B-209, ALUMINUM ALLOYS 5083 AND 6061

1 INTRODUCTION

Objective

The objective of this study is to use scanning electron microscopy (SEM) to establish and characterize the nature of fractures in engineering materials. This characterization is to be accomplished by laboratory simulation of those types of fracture modes and material embrittlements most commonly encountered in in-service failures. This report discusses a segment of the study covering fracture characteristics of one high-strength, low-alloy pipeline steel, one carbon steel, and two aluminum alloys.

Approach

The fracture characteristics of one high-strength, low-alloy pipeline steel (ASTM A-607, grade 65), one carbon structural steel (ASTM A-516, grade 70), and two structural aluminum alloys (ASTM B-209, alloys 5083 and 6061) were analyzed. The materials were fractured under tensile, fatigue, and impact loading conditions. The effects of hydrogen embrittlement on the steels' behavior when fractured under tensile and fatigue conditions were investigated.

Mode of Technology Transfer

The information obtained from examination of simulated failures will be combined with data gained from analysis of in-service failures to provide the basis for a reference manual to be used in future failure analysis.

Background

Fracture of Metals

Fracture surface features can be divided into two categories according to the mode of fracture: transgranular (through the grains and across grain boundaries) or intergranular (around the grain boundaries). Transgranular fractures can occur by void coalescence, rupture, cleavage, or fatigue. Intergranular fractures occur by grain boundary separation either with or without microvoid coalescence. Figures 1 through 4 illustrate these types of fractures in metals.

Many common structural metals fracture ductilely under monotonic load by microvoid coalescence. Microvoids are small, discontinuous voids which nucleate at grain boundaries, second-phase particles, or other sites where strain discontinuities exist. As the applied load increases, the microvoids grow, coalesce, and eventually form a continuous fracture surface which exhibits numerous cup-like depressions called "dimples"; this is referred to as "dimpled rupture," and is generally associated with ductile failure.

The shape of these dimples is strongly influenced by the orientation of the major stress axis in the individual grains and subgrains to the rolling direction of the material. Equiaxed dimples (Figure 1) result under local conditions of uniaxial tensile stress, while elongated dimples (Figure 2) result from failure caused by shear stress. Dimple size depends on the number of fracture nucleation sites, grain size, microstructure, and the relative ductility of the metal.

In polycrystalline body-centered cubic (bcc) metals, macroscopic cleavage fracture propagates through grains, changing directions as it crosses subgrain boundaries or passes from one grain to another. Cleavage fractures (Figure 3), which are usually associated with brittle failure, occur along a well-defined crystallographic plane within a grain; in ferritic steels which have a bcc crystal structure, this plane has the (100) type orientation. The change in orientation between grains and the imperfections within grains usually produce easily distinguished markings on the fracture surface. A cleavage fracture propagating across grains forms arrays of cleavage steps or "river patterns." These river patterns are rootlike networks of cleavage facets propagating on different levels.¹ In face-centered cubic metals such as aluminum, separation along well-defined planes has only been observed under certain conditions.²

Fatigue fracture results from continuous microscopic progression of a crack caused by the application of a cyclic load. The mechanism of fatigue crack initiation is believed to involve slip plane fracture caused by

¹R. Honda, *International Conference on Fracture*, Sendai, Japan (1965); and J. R. Low, Jr., B. L. Averbach, et al., *Fracture* (John Wiley, 1959), p 163.

²"Fractography and Atlas of Fractographs," *ASM Metals Handbook*, Vol 9, 8th ed. (American Society for Metals [ASM], 1974), p 65.

repetitive reversing of the operative slip systems on the surface of the metal.³ Crack growth caused by repetitive loading sometimes results in a fracture surface which exhibits closely spaced fatigue striations or parallel markings. Each fatigue striation represents the advance of a crack front during one loading cycle. The striations may be absent or may differ in appearance depending on such variables as type of material, level and frequency of applied stress, and environment.

Hydrogen Embrittlement of Steel

Hydrogen embrittlement has received considerable attention,⁴ since hydrogen is easily introduced into metals by melting, casting, welding, corrosion, and electroplating. However, most investigations of hydrogen embrittlement have been performed under sustained-load or slow strain rate tensile test conditions. Some research⁵ has been published on the fatigue properties of hydrogen-embrittled steels.

The degree of embrittlement generally increases with increasing hydrogen content and has the greatest effect on the high tensile-strength iron-base alloys.

Hydrogen embrittlement produces a sharp loss in ductility; this loss is most severe at room temperature and slow strain rates. The fatigue lives of steels subjected to electrolytic hydrogen-charging⁶ or a high-pressure hydrogen atmosphere⁷ have shown sig-

nificant reductions. The mode of failure of a hydrogen-embrittled sample depends on such variables as type of material, method of loading, and environment; martensitic steels are most susceptible.

Many theories concerning the mechanism of hydrogen embrittlement have been proposed, but no one theory has been able to account for more than half the experimental results. The hydrogen-embrittlement theory proposed by Zaffe⁸ was based on atomic hydrogen diffusing through the metal lattice, precipitating in internal voids as molecular hydrogen, and creating high pressures. It was assumed that high pressures in the voids, combined with the externally applied stress, fractured the metal. Diffusion of hydrogen to the voids could explain the strain rate and temperature dependence of hydrogen embrittlement; i.e., hydrogen embrittlement appears to be a rate process. However, this theory requires the presence of a regular array of pre-existing internal voids along with a source of hydrogen—a requirement that is inconsistent with the results of studies on the structure of hydrogen-embrittled steels.⁹ Petch¹⁰ rejected the idea that cracking is propagated by internal hydrogen pressure. He suggested that absorption of hydrogen on the surfaces of microcracks or voids reduces the surface free energy, resulting in a decrease in the energy needed for crack propagation. He further suggested that although plastic deformation may produce many disconnected microcracks, the microcracks do not reduce fracture stress significantly in the absence of hydrogen. However, when hydrogen is present, it diffuses into the region of the advancing tip and is absorbed at the crack tip, thereby reducing the energy required to propagate the crack. Troiano¹¹ has proposed that ionic hydrogen, which is evenly distributed throughout the metal lattice, is harmless because its concentration is so small. The critical factor is the segregation of hydrogen, which, under an applied stress, diffuses to regions of triaxial stress near pre-existing voids in the steel. Thus, only hydrogen in the stressed region of the lattice or at a crack tip is responsible for hydrogen embrittlement. Also, since hydrogen embrittlement is observed in

³P. J. E. Forsyth, "Fatigue Damage and Crack Growth in Aluminum Alloys," *ACTA Metallurgica*, Vol II (1963), p 703; and C. Laird and G. C. Smith, "Crack Propagation in High Stress Fatigue," *Philosophical Magazine*, Vol 2 (1962), p 847.

⁴P. Cotterill, "The Hydrogen Embrittlement of Metals," *Progressive Materials Science*, Vol 9, No. 4 (1961); A. S. Tetelman and A. J. McEvily, Jr., *Fracture of Structural Materials* (John Wiley, 1967); I. M. Bernstein, "The Role of Hydrogen in the Embrittlement of Iron and Steel," *Materials Science and Engineering*, Vol 6, No. 1 (1970), pp 1-19; W. Beck, E. J. Jankowski, and P. Fisher, *Hydrogen Stress Cracking of High-Strength Steels*, NADC-MA-7140 (Naval Air Development Center, 1971); and *Hydrogen Embrittlement Testing*, ASTM STP543 (American Society for Testing and Materials [ASTM], 1974).

⁵Y. G. Kim and J. Aleszka, *Fatigue Failure of Hydrogen-Embrittled High-Strength Steels*, Technical Report M-143/ADA013380 (Construction Engineering Research Laboratory, July 1975).

⁶G. Schwen, G. Sachs, and K. Tonk, *ASTM Proceedings*, Vol 57 (1957), pp 682-697; W. Beck, *Electrochemical Technology*, Vol 2 (1964), pp 74-78; and J. D. Harrison and G. C. Smith, *British Welding Journal*, Vol 14 (1967), pp 493-502.

⁷W. A. Spitzig, P. M. Talda, and R. P. Wei, "Fatigue-Crack Propagation and Fractographic Analysis of 18 Ni(250) Maraging Steel Tested in Argon and Hydrogen Environments," *Engineering Fracture Mechanics*, Vol 1 (1968), pp 155-165.

⁸C. A. Zaffe, *Journal of Iron and Steel Institute*, Vol 154, No. 123 (1946).

⁹A. S. Tetelman and A. J. McEvily, Jr., *Fracture of Structural Materials* (John Wiley, 1967).

¹⁰N. J. Petch, "The Ductile Fracture of Polycrystalline Iron," *Philosophical Magazine*, Vol 1 (1956), pp 186-191.

¹¹A. Troiano, "The Role of Hydrogen and Other Interstitials in the Mechanical Behavior of Metals," *Transactions of the American Society for Metals (ASM)*, Vol 52 (1960), p 52.

transitional metals having vacancies in the third subshell, Troiano hypothesized that hydrogen in the stressed region of the atomic lattices near the voids gives up its electrons to the third subshells of the host atoms, filling the vacancies in the third band, and thereby decreasing the binding energy of cohesiveness of the atoms in the lattice in this region. One flaw in this theory is that specimens slowly cooled in a hydrogen atmosphere or cathodically charged at room temperature contain cracks even without externally applied stress.

It should be noted that the deleterious effects associated with hydrogen can be removed by outgassing or "baking" the material for a short time in a temperature range of 100°C to 300°C.¹² At this temperature range, hydrogen readily diffuses to free surfaces and escapes as diatomic hydrogen.

¹²A. S. Tetelman and A. J. McEvily, Jr., *Fracture of Structural Materials* (John Wiley, 1967).

2 EXPERIMENTAL PROCEDURE

Material

Specimens of the ASTM A-516 and ASTM B-209, A1 alloys 5083 and 6061, were prepared from 1-in. (2.54-cm)-thick plates. The ASTM A-607 specimens were prepared from a 5/8-in. (1.59-cm)-thick pipe which had been cut and straightened. Type A-516 is a carbon steel intended primarily for use in welded pressure vessels where improved notch toughness is important. Its microstructure (Figure 5) consists of fine-grained ferrite. Type A-607 is a high-strength, low-alloy columbium and/or vanadium steel intended for use in structures where strength and savings in weight are important. Its as-received microstructure is fine-grained ferritic (Figure 6). Alloys 5083 and 6061 are structural aluminums used for sheet and plate. Their as-received structures are shown in Figures 7 and 8.

The chemical compositions, mechanical properties, and impact energies of the steels and aluminums are shown in Tables 1, 2, and 3, respectively.

Table 1
Chemical Composition of Materials

Element	ASTM A-516 grade 70, %	ASTM A-607 grade 65, %	ASTM A1 Alloy 5083, %	ASTM A1 Alloy 6061, %
Carbon	0.28 (max)	0.30 (max)	—	—
Manganese	0.80-1.25	1.55 (max)	0.40-1.0	0.15 (max)
Phosphorus	0.035 (max)	0.05 (max)	—	—
Sulfur	0.04 (max)	0.06 (max)	—	—
Silicon	0.13-0.33	—	0.40 (max)	0.4-0.8
Columbium	—	0.004 (min)	—	—
Nitrogen	—	0.015 (max)	—	—
Iron	—	—	0.40 (max)	0.7 (max)
Copper	—	—	0.10 (max)	0.15-0.40
Magnesium	—	—	4.0-4.9	0.8-1.2
Chromium	—	—	0.05-0.25	0.04-0.35
Zinc	—	—	0.25 (max)	0.25 (max)
Titanium	—	—	0.15 (max)	0.15 (max)
Other Elements	—	—	0.15 (max)	0.15 (max)
Aluminum	—	—	remainder	remainder

Table 2
Mechanical Properties of Steels and Aluminums

Material	Tensile Strength, ksi (MPa)	Yield Strength, ksi (MPa)
ASTM A-516	77 (531.3)	40.8 (281.5)
ASTM A-516, hydrogen-embrittled	78 (538.2)	42 (289.8)
ASTM A-607	89 (614.1)	81.2 (560.3)
ASTM A-607, hydrogen-embrittled	85.6 (590.6)	71.2 (491.3)
Aluminum 5083 alloy	41 (282.9)	31 (213.9)
Aluminum 6061 alloy	41 (282.9)	33 (227.7)

Table 3
Absorbed Impact Energies of Materials

Specimen	Testing Temperature, °C	Absorbed Energy, ft - lb (joule)
ASTM A-516	-196	2 (2.72)
ASTM A-516	0	189 (257.04)
ASTM A-516	25	178 (242.08)
ASTM A-516	100	172 (233.92)
ASTM A-607	-196	1.5 (2.04)
ASTM A-607	0	65 (88.4)
ASTM A-607	25	92 (125.12)
ASTM A-607	100	95 (129.2)
Aluminum 5083 alloy	-196	27 (36.72)
Aluminum 5083 alloy	0	17.5 (23.8)
Aluminum 5083 alloy	25	17.0 (23.12)
Aluminum 5083 alloy	100	17.0 (23.12)
Aluminum 6061 alloy	-196	12.0 (16.32)
Aluminum 6061 alloy	0	12.5 (17.00)
Aluminum 6061 alloy	25	13.0 (17.68)
Aluminum 6061 alloy	100	15.5 (21.08)

Specimen Fabrication and Testing

Figure 9 shows the specimen geometry for the tensile, impact, and fatigue tests. The specimens were machined with the specimens' longitudinal axes parallel to the rolling direction.

The tensile tests were conducted at room temperature at strain rates between 0.01 in./in./min. (0.01 cm/cm/min.) and 0.06 in./in./min (0.06 cm/cm/min.), using a 50-kip MTS electrohydraulic testing machine. The impact specimens, which were the Charpy V-notched type, were tested at a range of temperatures by using temperature control baths. The fatigue tests for the specimens were conducted at 10 cycles/sec in a tension/tension sinusoidal mode at room temperature (23°C) using a 50-kip MTS unit.

Hydrogen Embrittlement

To induce hydrogen embrittlement, specimens were cathodically charged in a solution of 10 weight percent H₂SO₄ and 0.3 weight percent As₂O₃. The As₂O₃ was used to promote absorption of hydrogen during cathodic polarization. The cathodic charging was conducted at a current density of 6 ma/in.² (0.93 ma/cm²) for 12 hours.

3 RESULTS AND DISCUSSION

Summaries of the mechanical tests conducted in this study are shown in Tables 2 and 3.

ASTM A-516 Steel

The fracture surface of the A-516 tensile sample is shown in Figure 10. Failure occurred by inclusion-generated dimple rupture. Figure 11 shows various dimple sizes and a large inclusion.

Regions of fatigue and tensile overload can be identified on the fracture surface of the A-516 fatigue specimen (Figure 12). Failure in the tensile overload regions occurred by dimple rupture which initiated at inclusions (Figure 13). Failure in the fatigue regions consisted primarily of transgranular fracture (Figure 14).

The fracture surfaces of the hydrogen-embrittled A-516 tensile (Figure 15) and fatigue (Figure 16) specimens were very similar to the unembrittled tensile and fatigue specimens. Failure in the hydrogen-embrittled tensile specimen occurred by inclusion-generated dimple rupture (Figure 17). A fractured pearlite colony can also be identified on this fracture surface. Regions of tensile overload and fatigue were found on the hydrogen-embrittled fatigue specimen surface. Failure occurred by dimple rupture in the tensile overload region and by transgranular fracture in the fatigue region. Some areas of fatigue striae were found in the fatigue region; the fatigue striae indicate a stepwise, cyclic progression of the crack front across the fracture surface (Figure 18).

Figure 19 shows the fracture surface of an as-received ASTM A-516 Charpy impact specimen tested to failure at -196°C. A higher magnification of the surface (Figure 20) shows that failure occurred by cleavage. Numerous "river patterns," which represent steps between different local cleavage facets of the same general cleavage plane, can be identified on the fracture surface. The impact specimens tested at 0, 25, and 100°C (Figures 21, 22, and 23) exhibited lamellar tearing caused by the presence of "stringers" (elongated inclusions) in the steel oriented perpendicular to the crack plane. As a result of these inclusions, the specimens were extremely tough and did not break completely. Another possible reason is that the transition temperature for this material is below 0°C, with the result that the energy responses fell on the upper shelf of the energy-temperature curve. Also, the Charpy V-notch specimen in many cases does not have the necessary geometry to contain the plastic deformation zone which precedes the crack. The unnotched portion of the Charpy may have a dimension less than the ratio of K_{Ic} (stress-intensity) to yield strength. These latter factors will lead to high energy absorption values.

Photographs, rather than SEM photomicrographs, are shown of these specimens.

ASTM A-607 Steel

The surface of the as-received ASTM A-607 tensile specimen in Figure 24 indicates a ductile fracture. Failure occurred by inclusion-generated dimple rupture. Figure 25 shows a higher magnification of a typical region of dimple rupture.

The fracture surface of the as-received ASTM A-607 fatigue specimen shows a large fatigue region on one side, a very small tensile overload region, and a very small fatigue region on the other side (Figure 26). There is evidence of two inclusions on the side with the large fatigue region, indicating that rapid initiation of fatigue was caused by increased stress induced by the inclusions. The fatigue region failed by transgranular fracture in which areas of fatigue striae could be identified (Figure 27). Failure occurred by dimple rupture in the tensile overload region.

The hydrogen-embrittled ASTM A-607 tensile specimen (Figure 28) demonstrated less plastic deformation than the unembrittled tensile specimen (Figure 24). There was less reduction in the cross-sectional dimensions in the hydrogen-embrittled specimen, and the dimples were somewhat flatter than in the unembrittled sample.

The hydrogen-embrittled fatigue specimen (Figure 29) showed the large region of fatigue on one side, again indicative of an inclusion initiating rapid fatigue. More distinct fatigue striae are seen in the hydrogen-embrittled sample (Figure 30) than in the unembrittled sample.

The as-received ASTM A-607 Charpy impact specimens showed increasing plastic deformation with increasing testing temperature. Failure occurred by cleavage in the -196°C specimen (Figures 31 and 32), and by dimple rupture in the higher temperature specimens (Figures 33 through 38). The dimple rupture and increase in shear lip size with increasing testing temperature is evidence of the increasing plastic deformation and increasing ductility.

ASTM B-209, Aluminum Alloy 5083

The failure of the as-received aluminum 5083 tensile specimen was very ductile, producing an extremely slanted fracture surface (Figure 39). A higher magnification of the surface (Figure 40) shows an elongated dimple rupture structure.

The fracture surface of the as-received aluminum 5083 specimen shows the typical regions of tensile overload and fatigue (Figure 41). Failure occurred by inclusion-generated dimple rupture in the tensile overload region (Figure 42). The fatigue region shows very definite regions of fatigue striae, as shown in Figures 43 and 44.

The aluminum 5083 Charpy impact specimens all failed in a ductile manner. The -196°C specimen had a very slanted surface whose layers indicated tearing along the grain structure (Figure 45). This is the result of large amounts of second phases congregating in the grain boundaries as shown in the microstructure in Figure 7. At this low temperature, the failure propagates through the less cohesive grain boundaries. The remaining specimens have a fibrous appearance indicating some influence of grain boundary tearing (Figures 46, 47, and 48). Failure occurs primarily by dimple rupture, and the surfaces indicate increasing plastic deformation as demonstrated by increasing shear lip size.

ASTM B-209, Aluminum Alloy 6061

The fracture surface of the aluminum 6061 tensile specimen is shown in Figure 49. Failure occurred by inclusion-generated dimple rupture (Figure 50). Alloy 6061 is a precipitation-hardened aluminum in which precipitates tie up dislocations and improve the material's yield strength. The effects of the different sizes of precipitates (inclusions) are shown very clearly in this alloy. Very fine dimples are formed around small inclusions; large dimples are formed around large inclusions.

The as-received aluminum 6061 fatigue specimen shows the typical tensile overload and fatigue regions (Figure 51). Failure occurred by inclusion-generated dimple rupture (Figure 52); the presence of both a fine and coarse dimple structure is also evident in this specimen. Failure in the fatigue region occurred by transgranular fracture, and areas of fatigue striae can be identified (Figure 53).

Failure occurred by dimple rupture in the as-received aluminum 6061 Charpy impact specimens tested at all temperatures (Figures 54 through 58). An increase in plastic deformation was evidenced by increasingly prominent shear lips with increasing testing temperature. However, in contrast to steel, and on the basis of absorbed energies, these alloys do not develop a ductile-to-brittle transition.

4 CONCLUSIONS

1. The presence of fatigue striae on the ASTM A-516 steel hydrogen-embrittled fatigue specimen that were not noted on the unembrittled fatigue specimen indicated that hydrogen embrittlement has some effect on the microstructure of the ASTM A-516 steel. The effect is assumed to be small, however, since the mechanical strength of the steel was not significantly altered.

2. The ASTM A-516 Charpy specimens were extremely tough in the orientation in which they were machined due to the presence of elongated inclusions perpendicular to the crack plane created by rolling.

3. The ASTM A-607 hydrogen-embrittled fatigue specimen showed more areas of fatigue striae than the unembrittled specimen, again indicating the effect of hydrogen embrittlement on the microstructure of the steel. The data demonstrate that the A-607 steel tested had superior tensile properties to those of the A-516 steel tested.

4. The effect of testing temperature on the ASTM A-607 Charpy specimens was seen in a change from low-energy, brittle fracture (primarily cleavage) at low temperatures to higher energy, ductile fracture (primarily dimple rupture) at elevated temperatures. Data also indicate that A-516 has superior Charpy V-notch properties compared to those of A-607 steel.

5. The aluminum 5083 alloy specimens produced very ductile failures. Very well-defined striae were observed in the fatigue specimen. The Charpy specimens all failed by dimple rupture, and the amount of plastic deformation increased with increased testing temperature. These alloys do not exhibit a ductile-to-brittle transition.

6. The effect of precipitates in the precipitation-hardened aluminum 6061 alloy is very evident in the areas of dimple rupture, where a coarse and fine dimple structure is observed around different-sized inclusions. Well-defined areas of fatigue striae are seen on the fatigue specimen. The Charpy specimens all failed by dimple rupture, and the amount of plastic deformation increased with increased testing temperature. These alloys do not exhibit a ductile-to-brittle transition.

REFERENCES

- Beck, W., E. J. Jankowski, and P. Fisher, *Hydrogen Stress Cracking of High-Strength Steels*, NADC-MA-7140 (Naval Air Development Center, 1971).
- Beck, W., *Electrochemical Technology*, Vol 2 (1964), pp 74-78.
- Bernstein, I. M., "The Role of Hydrogen in the Embrittlement of Iron and Steel," *Materials Science and Engineering*, Vol 6, No. 1 (1970), pp 1-19.
- Cotterill, P., "The Hydrogen Embrittlement of Metals," *Progressive Materials Science*, Vol 9, No. 4 (1961).
- Forsyth, P. J. E., "Fatigue Damage and Crack Growth in Aluminum Alloys," *ACTA Metallurgica*, Vol II (1963), p 703.
- "Fractography and Atlas of Fractographs," *ASM Metals Handbook*, Vol 9, 8th ed. (American Society for Metals [ASM], 1974), p 65.
- Harrison, J. D. and G. C. Smith, *British Welding Journal*, Vol 14 (1967), pp 493-502.
- Honda, R., *International Conference on Fracture*, Sendai, Japan (1965).
- Hydrogen Embrittlement Testing*, ASTM STP543 (American Society for Testing and Materials [ASTM], 1974).
- Kim, Y. G. and J. Aleszka, *Fatigue Failure of Hydrogen-Embrittled High-Strength Steels*, Technical Report M-143/ADA013380 (Construction Engineering Research Laboratory, July 1975).
- Laird, C. and G. C. Smith, "Crack Propagation in High Stress Fatigue," *Philosophical Magazine*, Vol 2 (1962), p 847.
- Low, J. R., Jr., B. L. Averbach, et al., *Fracture* (John Wiley, 1959), p 163.
- Petch, N. J., "The Ductile Fracture of Polycrystalline Iron," *Philosophical Magazine*, Vol 1 (1956), pp 186-191.

Schwen, G., G. Sachs, and K. Tonk, *ASTM Proceedings*, Vol 57 (1957), pp 682-697.

Spitzig, W. A., P. M. Talda, and R. P. Wei, "Fatigue-Crack Propagation and Fractographic Analysis of 18 Ni(250) Maraging Steel Tested in Argon and Hydrogen Environments," *Engineering Fracture Mechanics*, Vol 1 (1968), pp 155-165.

Tetelman, A. S. and A. J. McEvily, Jr., *Fracture of Structural Materials* (John Wiley, 1967).

Troiano, A., "The Role of Hydrogen and Other Interstitials in the Mechanical Behavior of Metals," *Transactions of the American Society for Metals (ASM)*, Vol 52 (1960), p 52.

Zaffe, C. A., *Journal of Iron and Steel Institute*, Vol 154, No. 123 (1946).

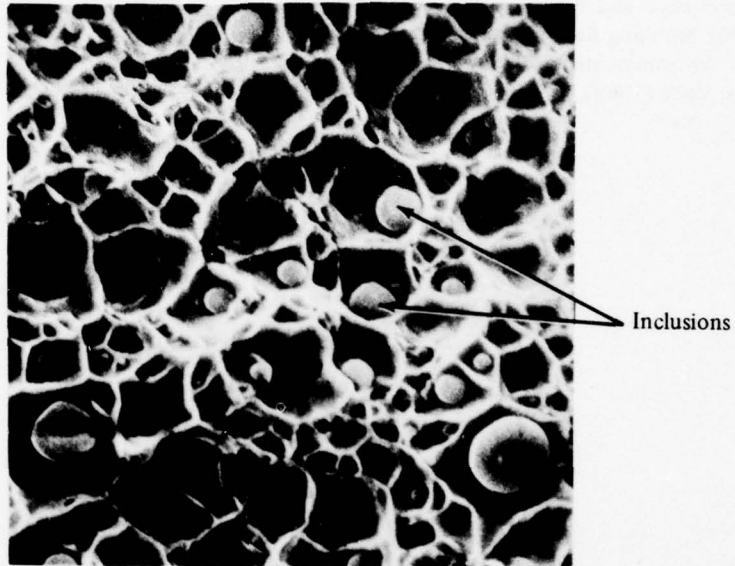


Figure 1. Typical equiaxed dimple structure containing inclusions, 4250X.

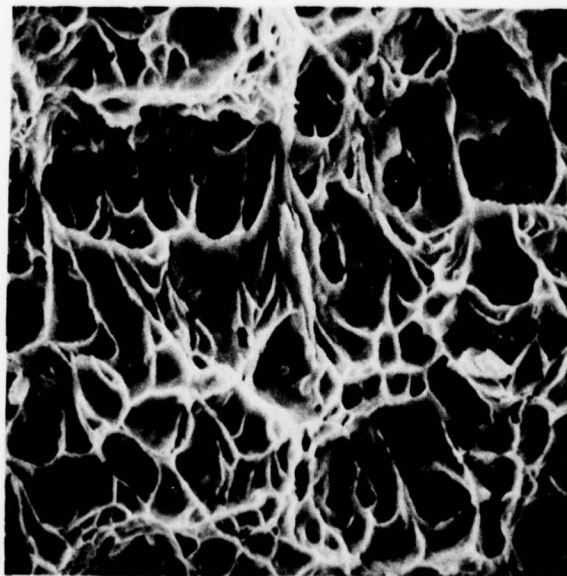


Figure 2. Typical elongated dimple structure, 3750X.



Figure 3. Typical cleavage facets, 400X.

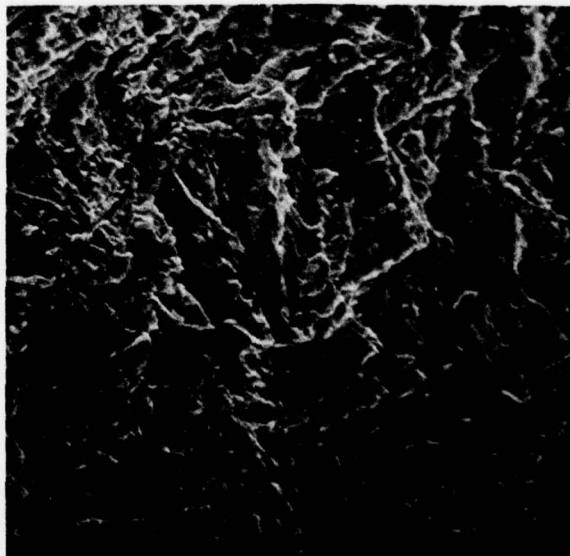


Figure 4. Typical fatigue striations, 4000X.



Figure 5. Microstructure of ASTM A-516 steel, 320X.

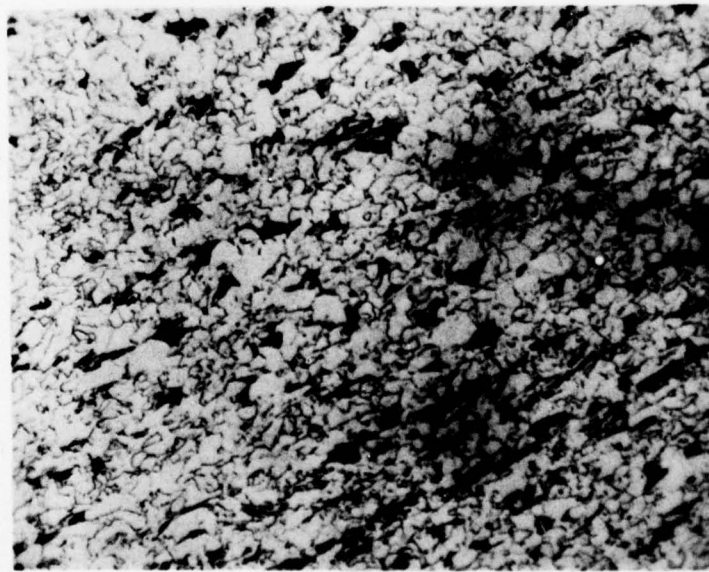


Figure 6. Microstructure of ASTM A-607 steel.

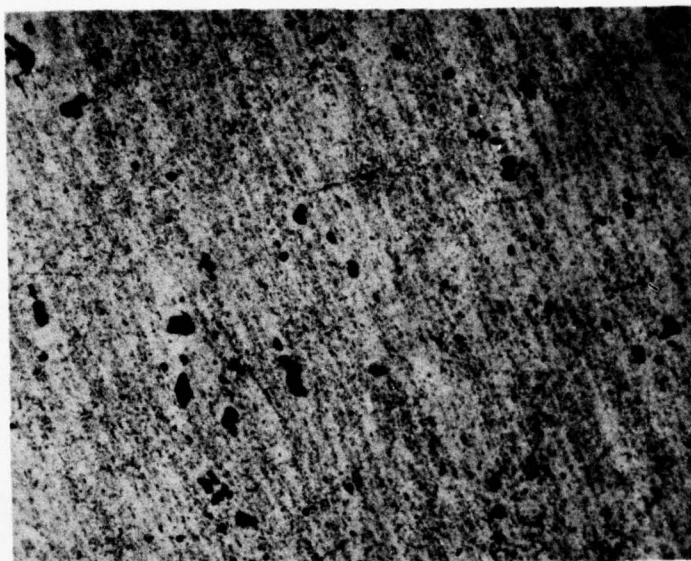


Figure 7. Microstructure of ASTM B-209, A1 alloy 5083.

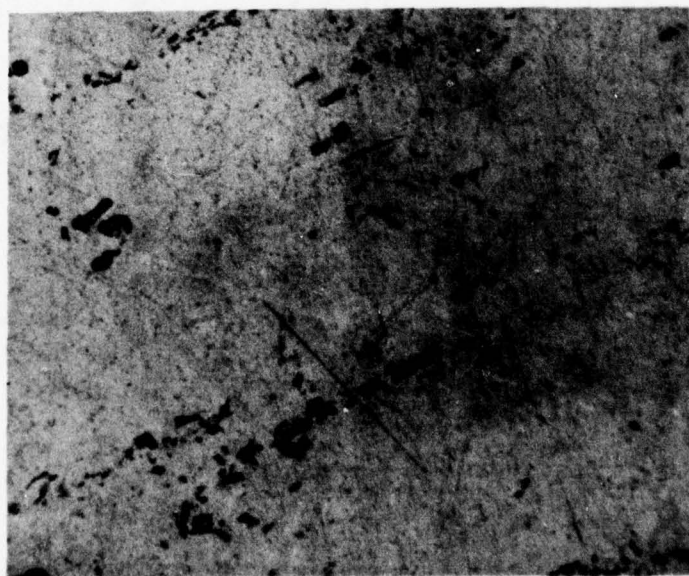
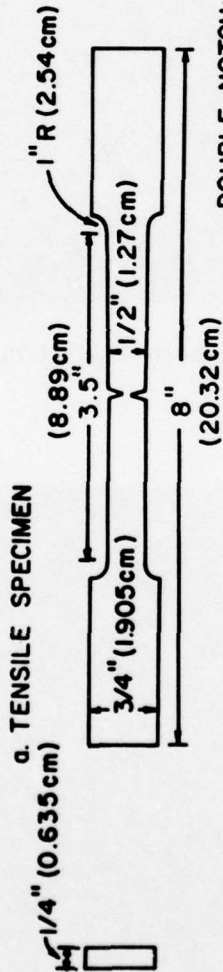
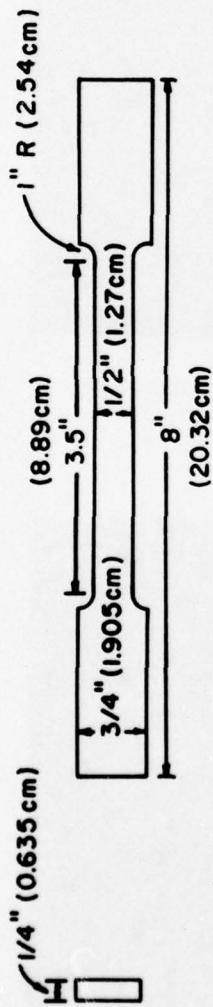
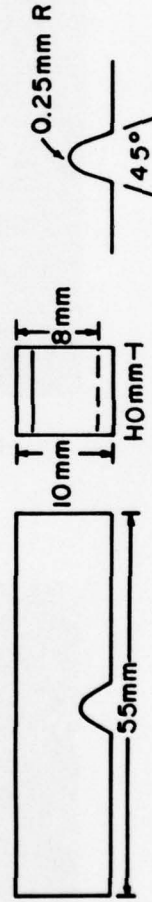


Figure 8. Microstructure of ASTM B-209, A1 alloy 6061.



DOUBLE NOTCH: 45°
 .001 IN. ROOT RADIUS (0.254 mm)
 1/8 IN. DEEP (3.175 mm)

b. FATIGUE SPECIMEN



c. CHARPY SPECIMEN

Figure 9. Specimen geometry for tensile, fatigue, and Charpy impact tests.

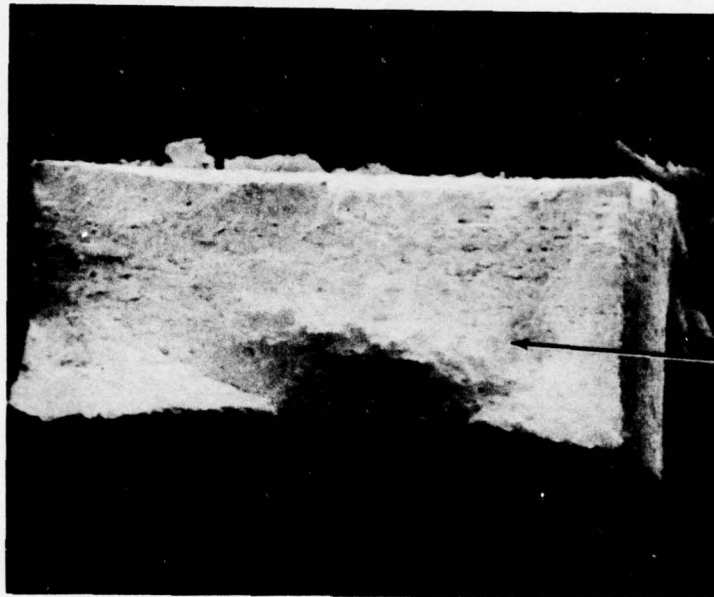
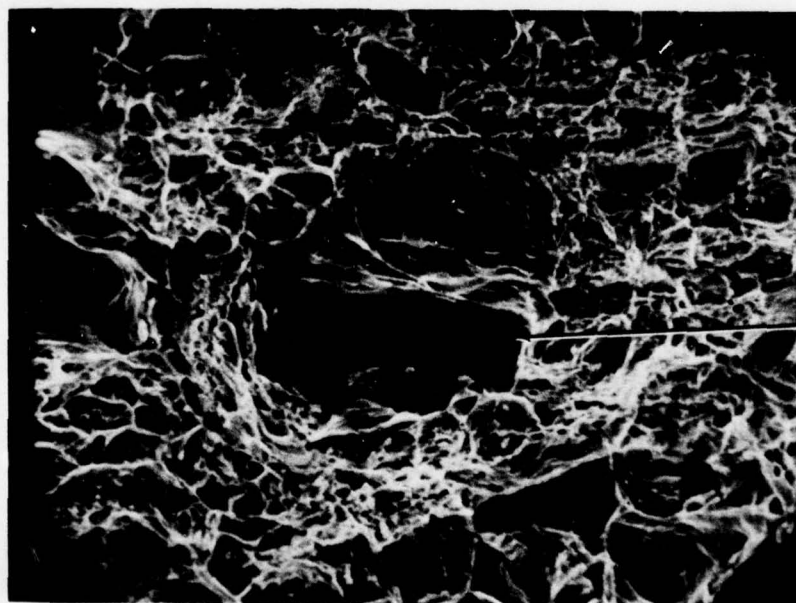


Figure 11

Figure 10. Tensile fracture surface of A-516 steel, 12X.



Inclusion

Figure 11. Dimple rupture in A-516 steel, 1200X.

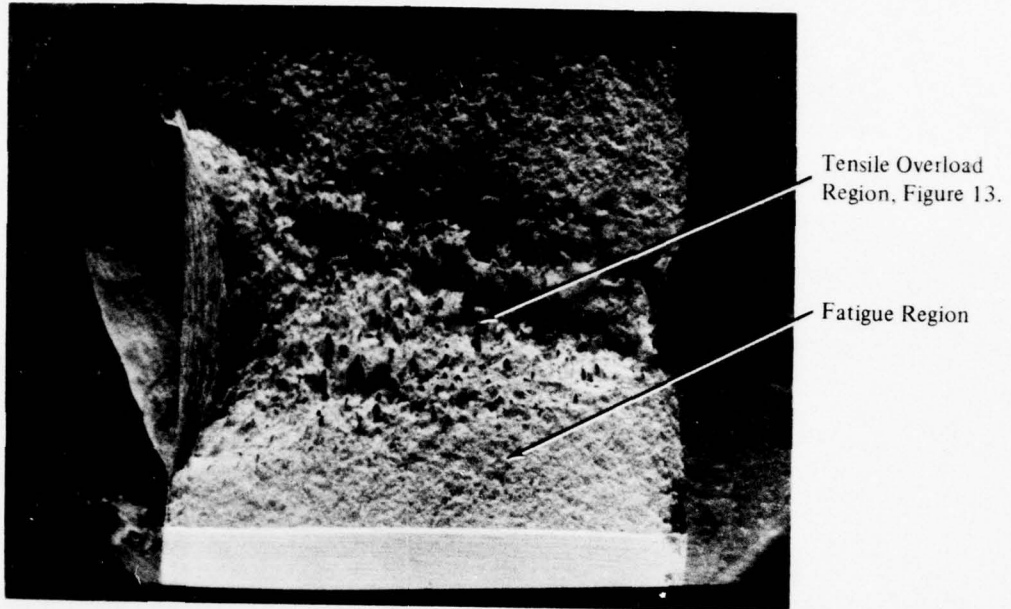


Figure 12. Fatigue fracture surface of A-516 steel, 8X.

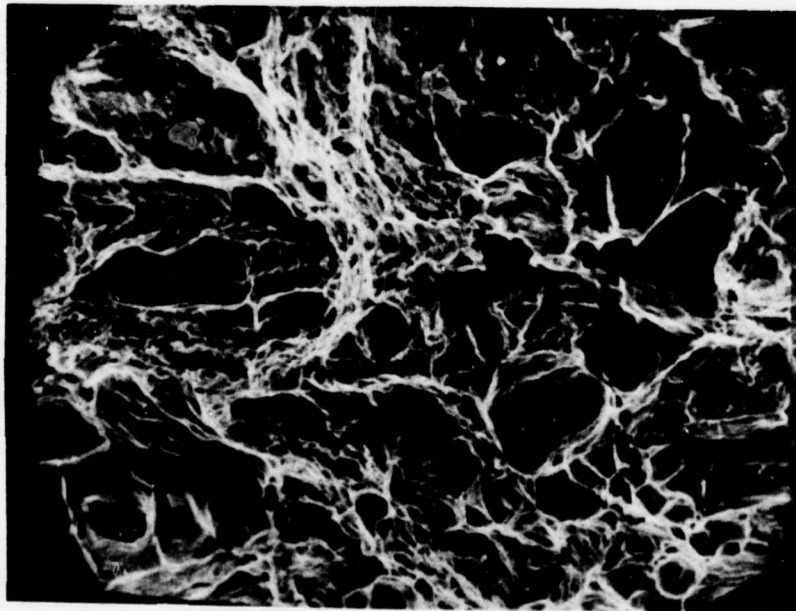


Figure 13. Dimple rupture in an A-516 fatigue specimen, 1000X.



Fatigue Striae

Figure 14. Transgranular fracture in an A-516 fatigue specimen, 650X.

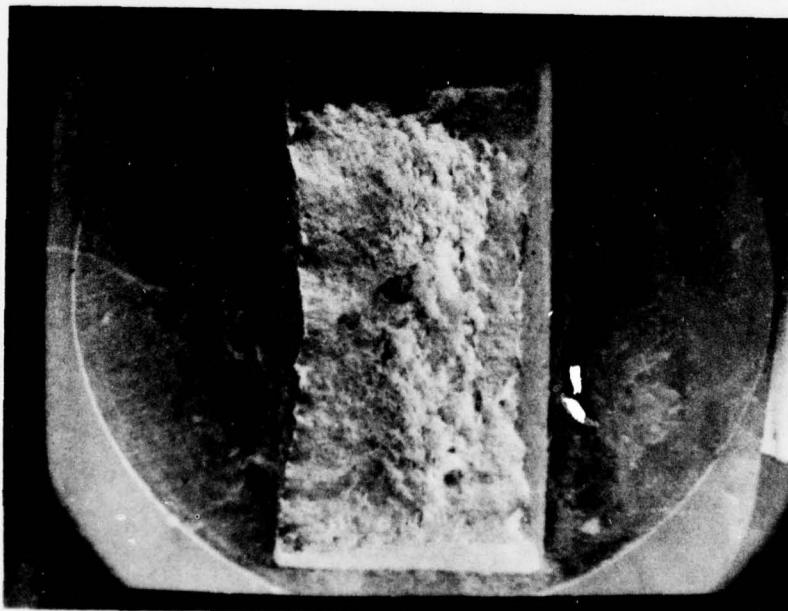
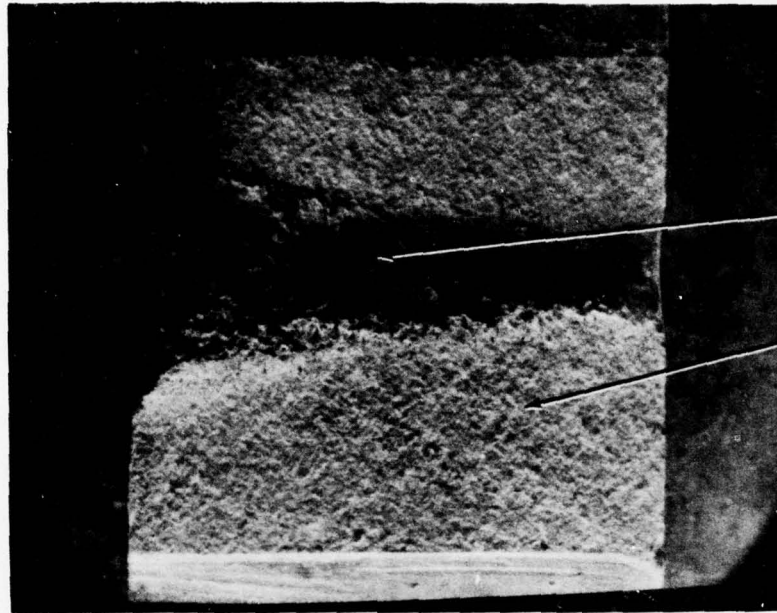


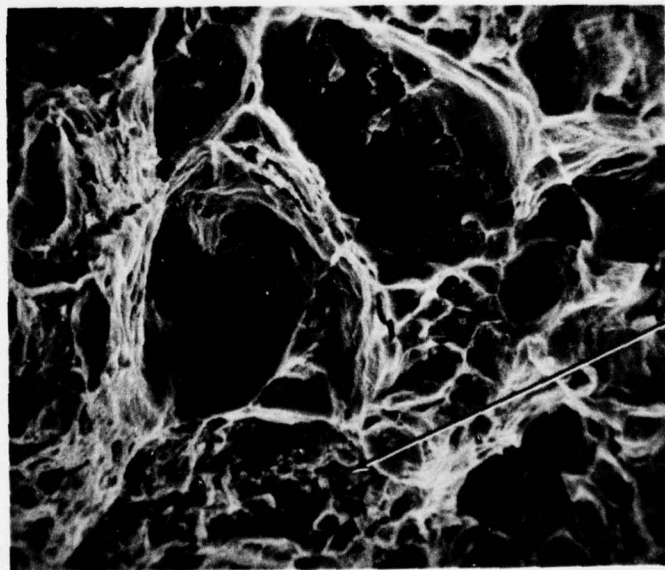
Figure 15. Tensile fracture surface of hydrogen-embrittled A-516 steel, 11X.



Tensile Overload
Region, Figure 17.

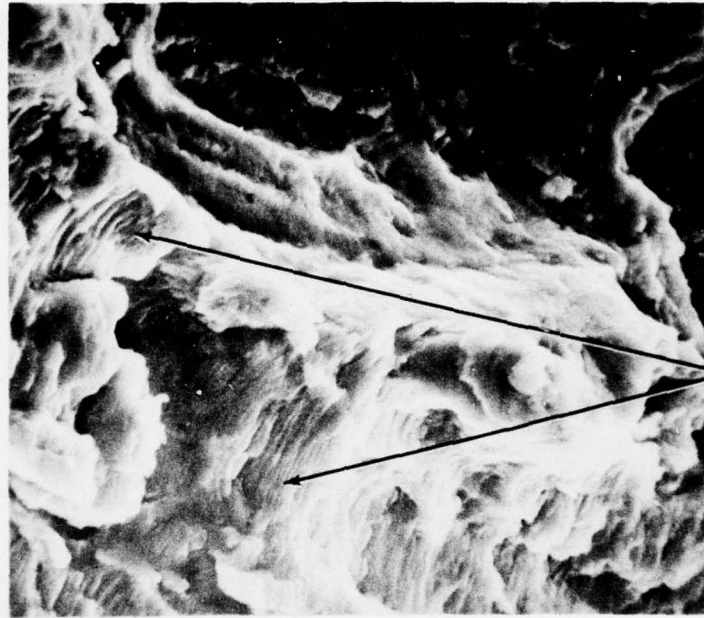
Fatigue Region,
Figure 18.

Figure 16. Fatigue fracture surface of hydrogen-embrittled A-516 steel, 12X.



Fractured Pearlite
Colonies.

Figure 17. Dimple rupture in a hydrogen-embrittled A-516 steel, 800X.



Fatigue Striations

Figure 18. Fatigue striations in A-516 steel, 1800X.

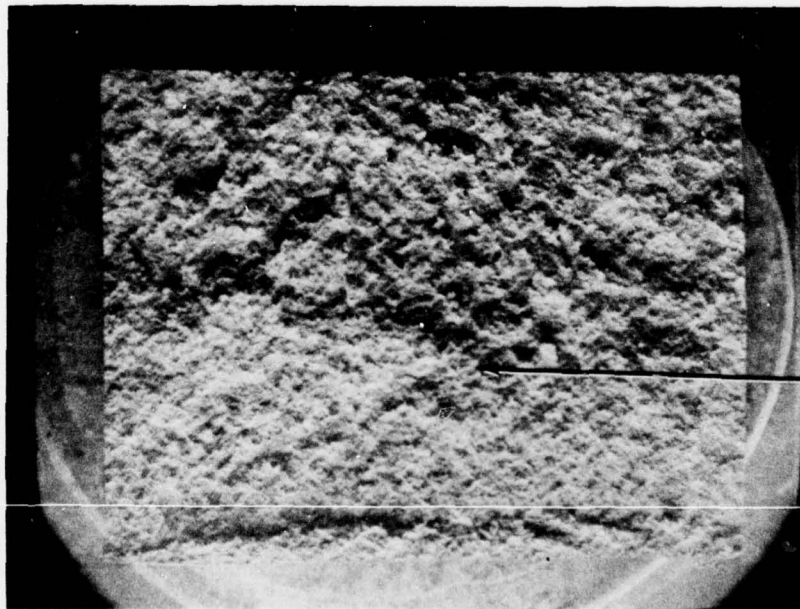


Figure 20

Figure 19. Fracture surface of an A-516 Charpy specimen tested at -196°C , 11X.

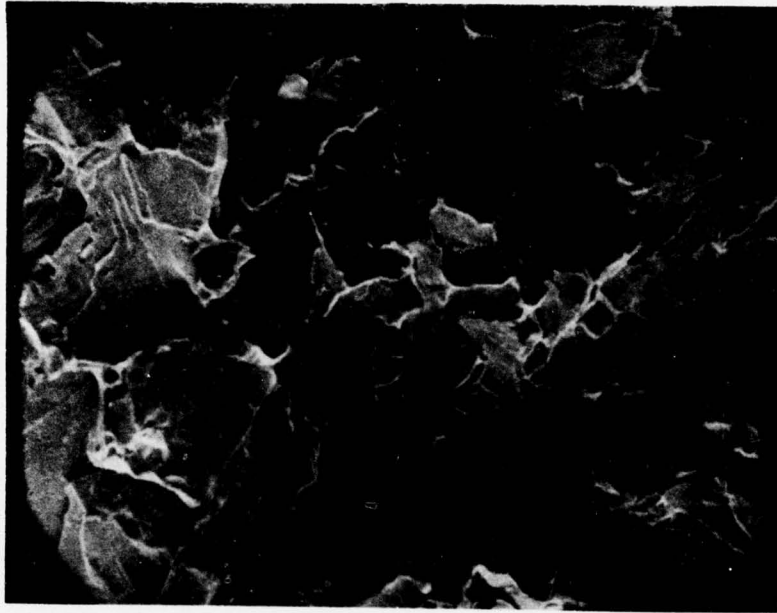


Figure 20. Cleavage facets in an A-516 Charpy specimen tested at -196°C , 550X.

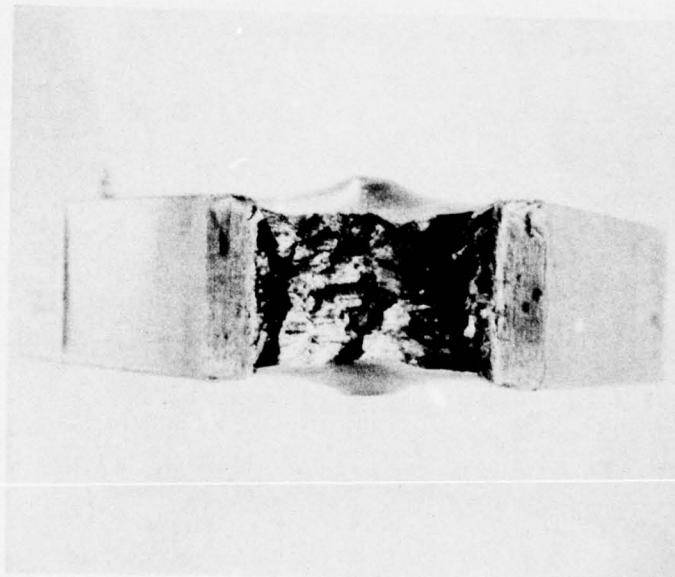


Figure 21. A-516 steel Charpy impact specimen tested at 0°C , 11X.

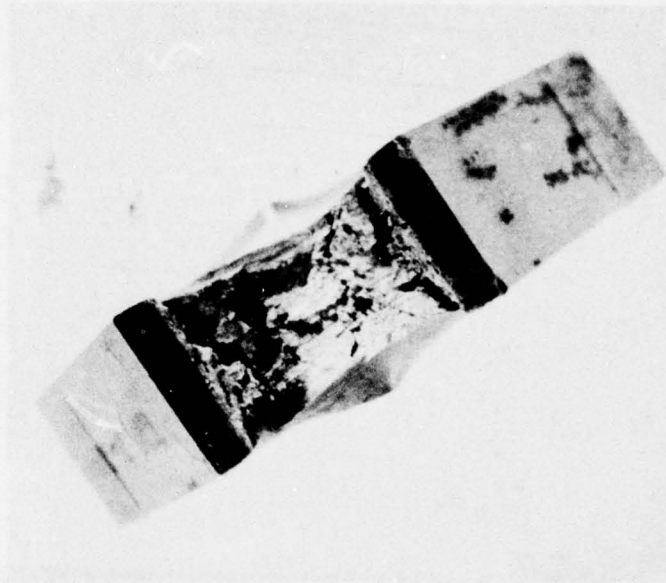


Figure 22. A-516 steel Charpy impact specimen tested at 25°C, 11X.

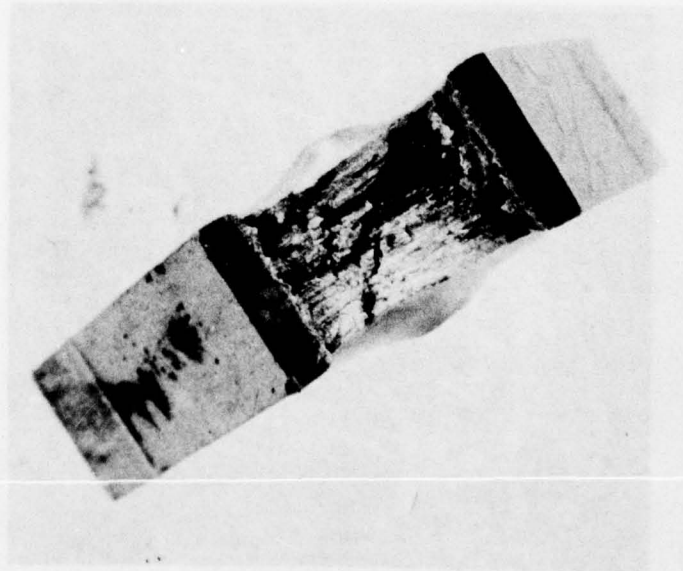


Figure 23. A-516 steel Charpy impact specimen tested at 100°C, 11X.

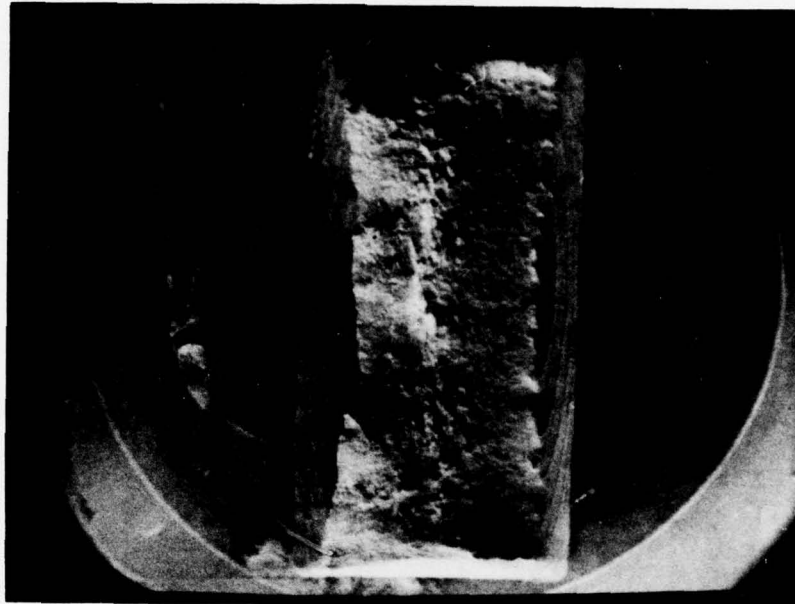


Figure 24. Tensile fracture surface of A-607 steel, 11X.

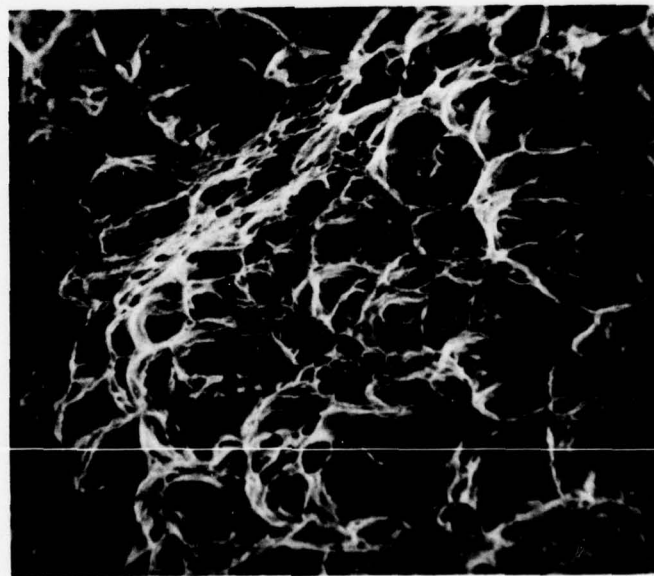


Figure 25. Dimple rupture in A-607 steel, 800X.

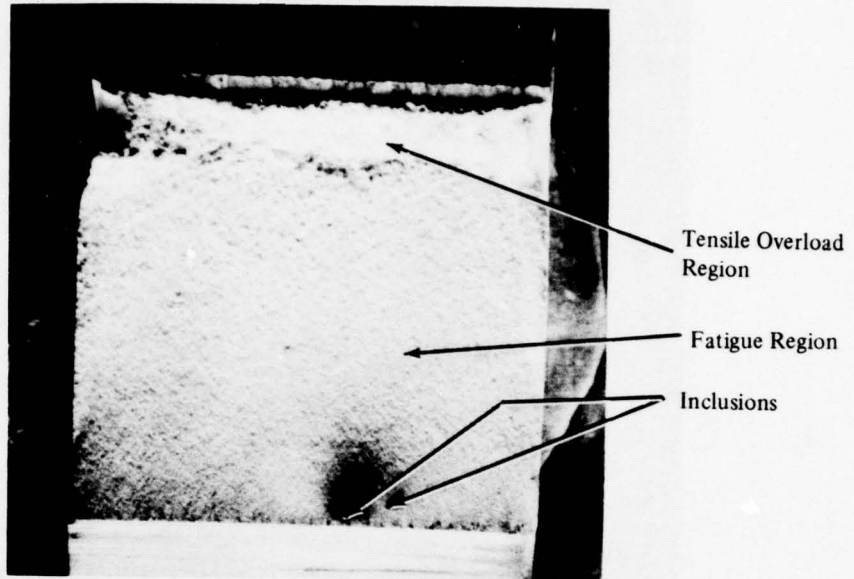


Figure 26. Fatigue fracture surface of A-607 steel, 12X.

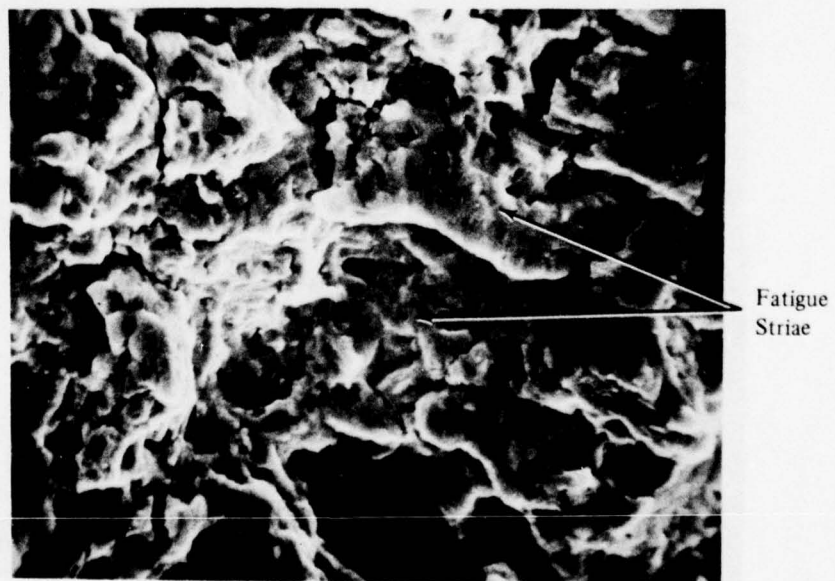


Figure 27. Fatigue striations in A-607 steel, 1000X.

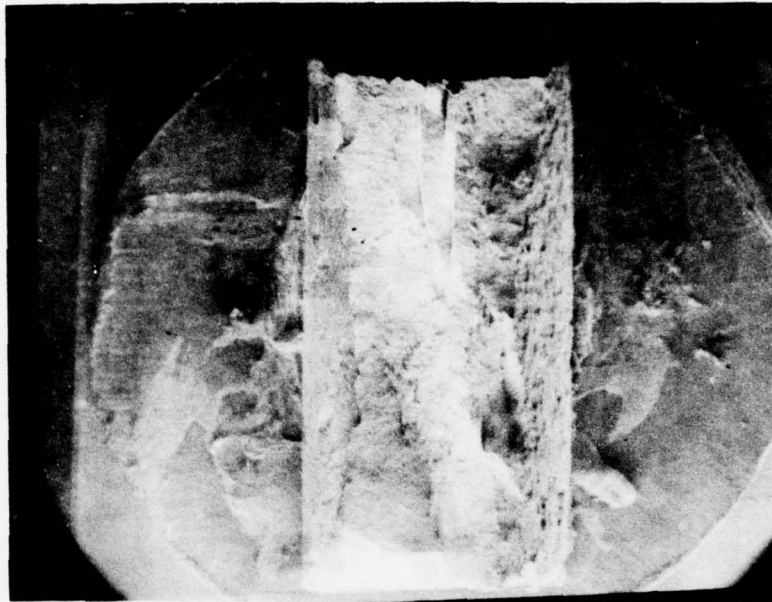


Figure 28. Hydrogen-embrittled tensile A-607 steel specimen, 11X.

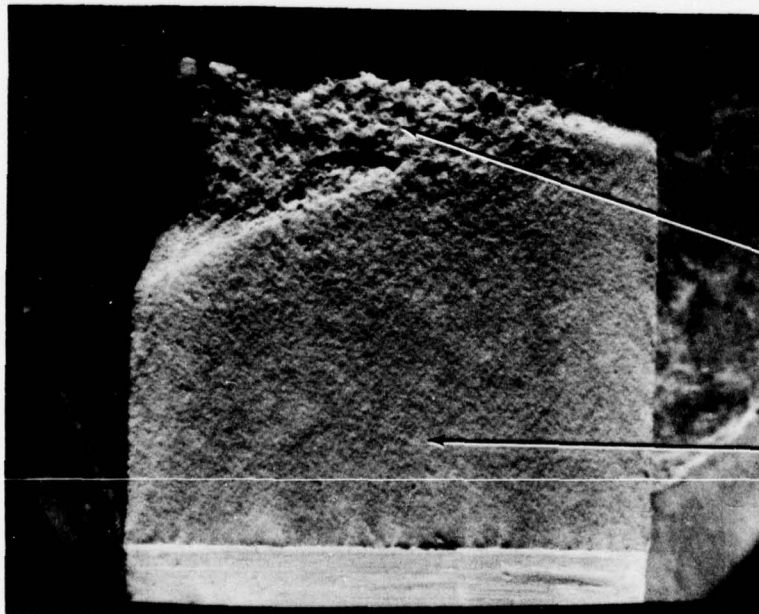
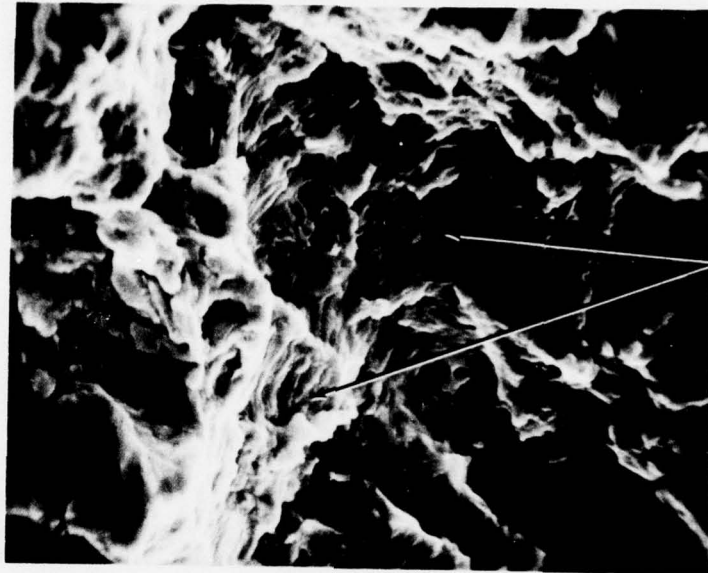


Figure 29. Hydrogen-embrittled fatigue A-607 steel specimen, 12X.



Fatigue
Striae

Figure 30. Fatigue striae in a hydrogen-embrittled A-607 steel specimen, 1000 X.

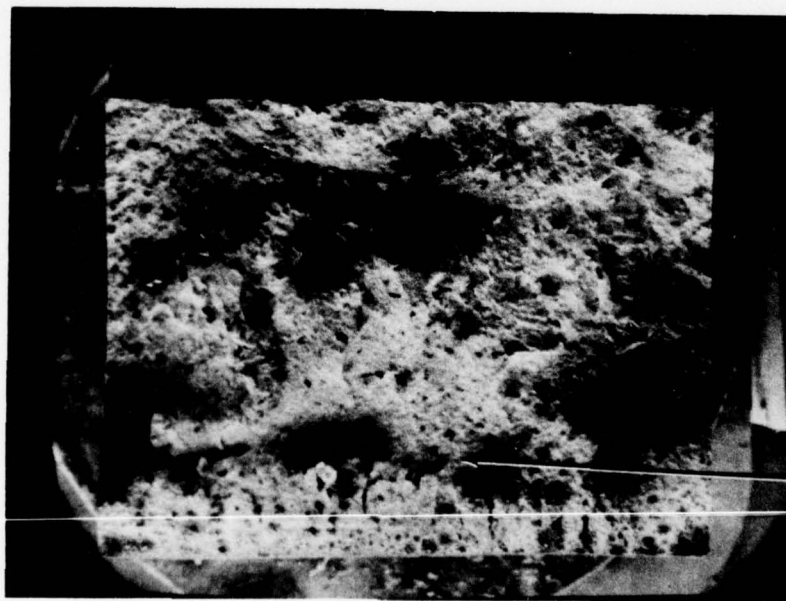


Figure 32

Figure 31. A-607 Charpy impact specimen tested at -196°C , 11X.

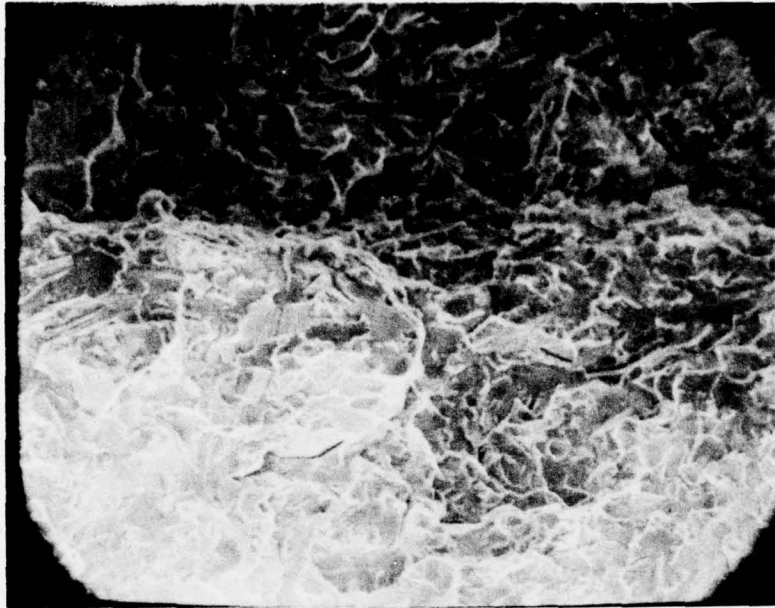


Figure 32. Cleavage facets in an A-607 Charpy impact specimen tested at -196°C , 550X.



Figure 34

Figure 33. A-607 Charpy impact specimen tested at 0°C , 9X.

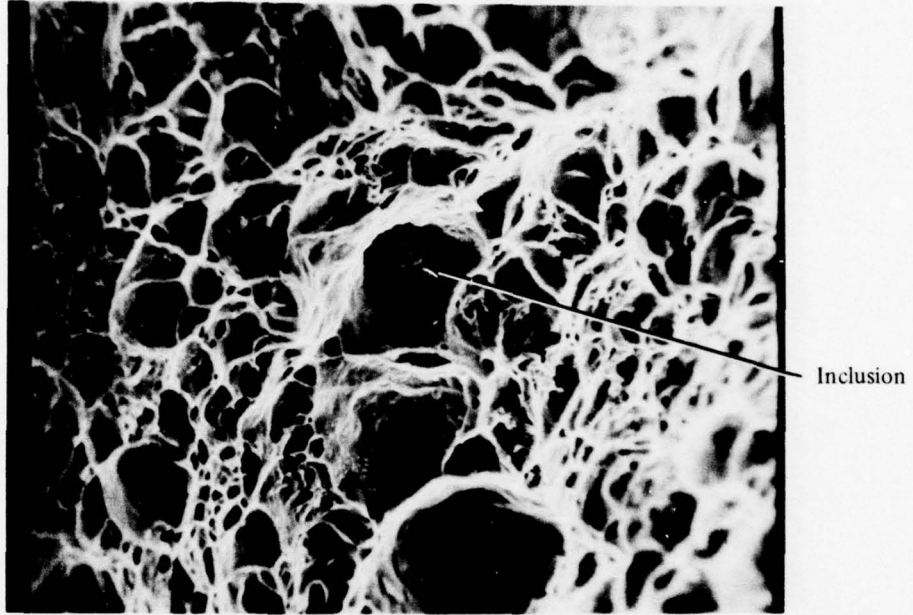


Figure 34. Dimple rupture in an A-607 Charpy impact specimen tested at 0°C, 300X.

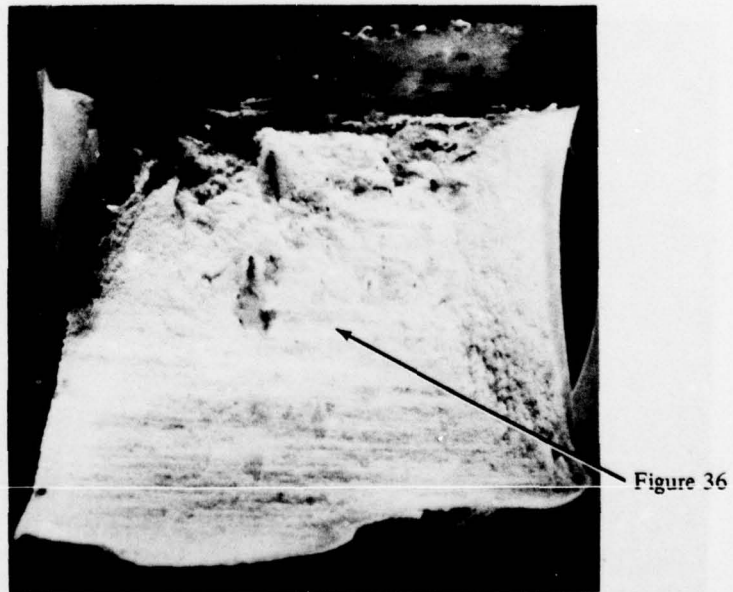


Figure 35. A-607 Charpy impact specimen tested at 25°C, 10X.

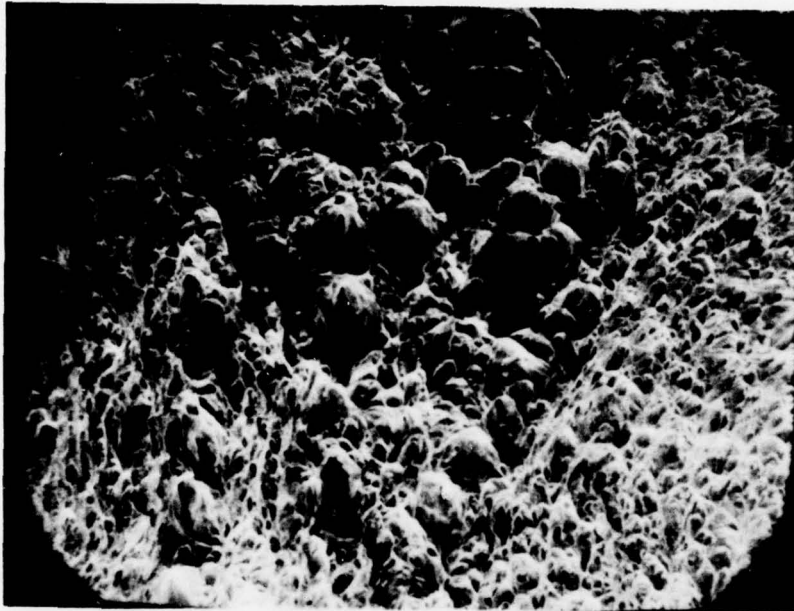


Figure 36. Dimple rupture in an A-607 Charpy impact specimen tested at 25°C, 250X.

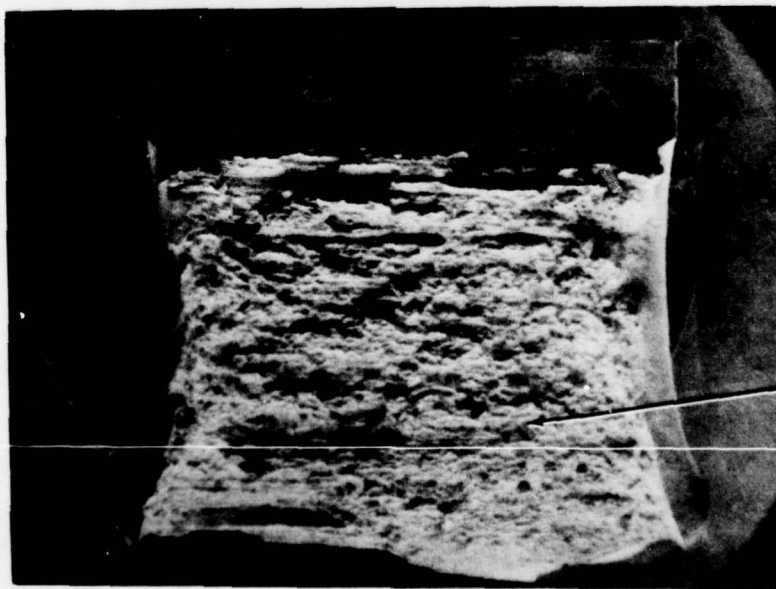
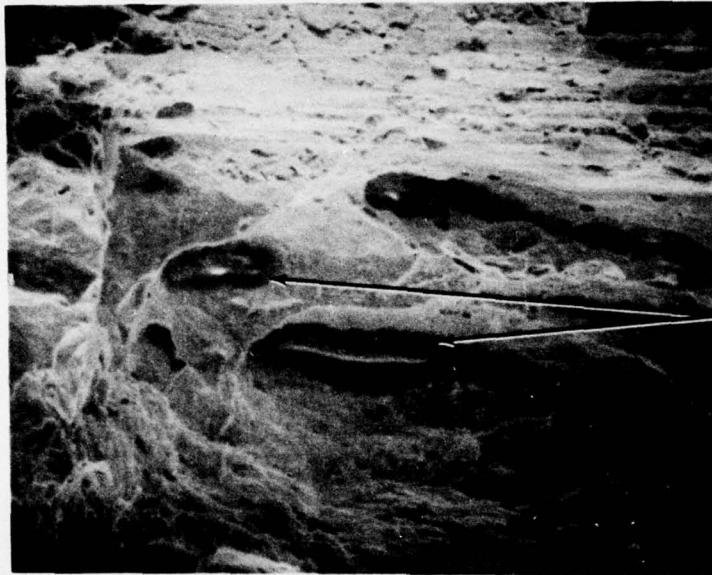


Figure 38

Figure 37. A-607 Charpy impact specimen tested at 100°C, 10X.



Inclusions

Figure 38. Dimple rupture and a large inclusion in an A-607 Charpy impact specimen tested at 100°C, 500X.

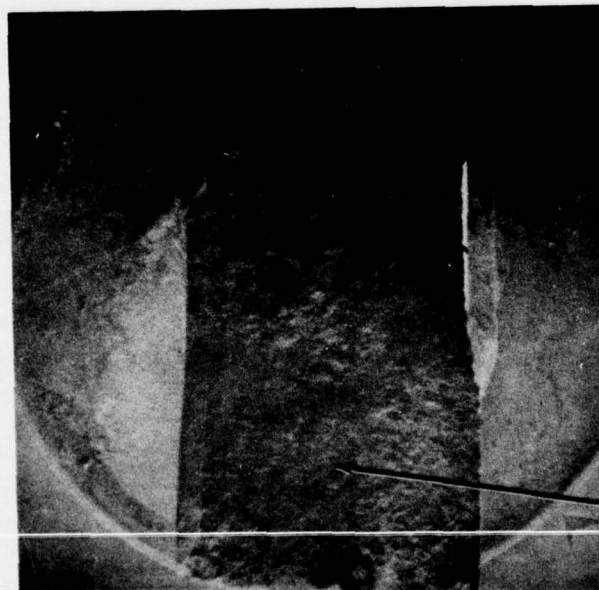


Figure 40

Figure 39. Tensile fracture surface of a 5083 aluminum specimen, 9X.

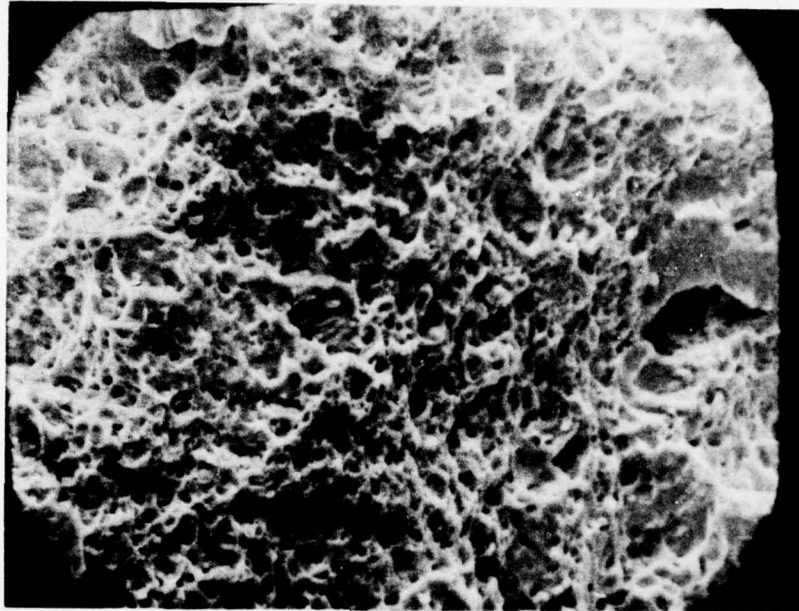


Figure 40. Dimple rupture in 5083 aluminum, 450X.

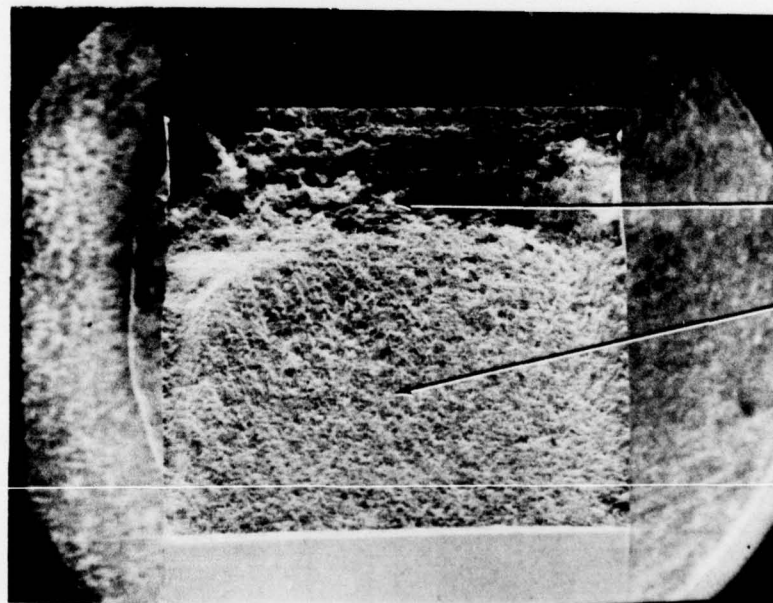


Figure 41. Fracture surface of 5083 aluminum tensile specimen, 12X.

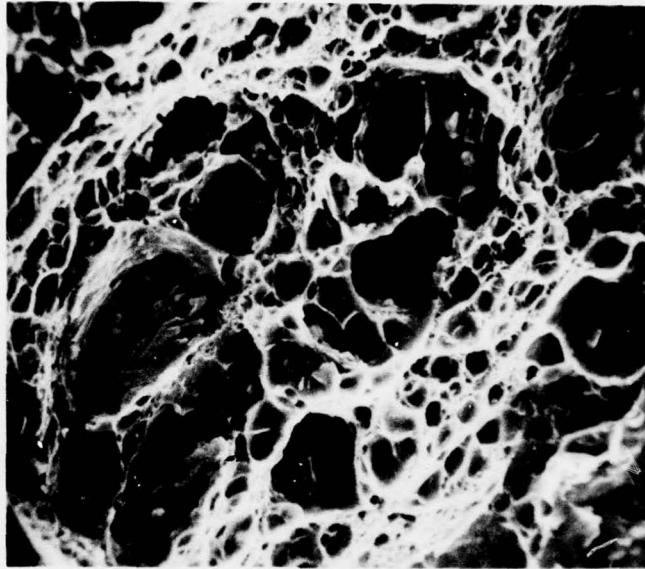


Figure 42. Dimple rupture in 5083 aluminum, 300X.

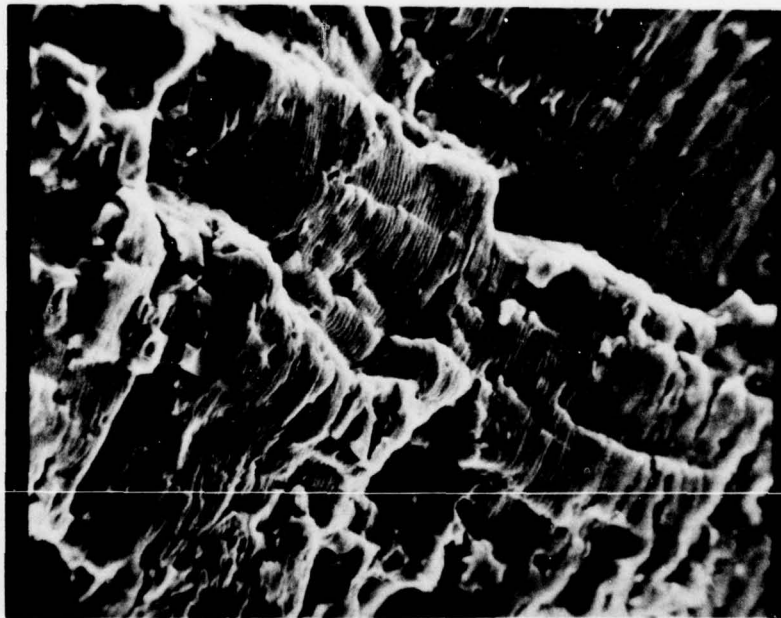


Figure 43. Fatigue striae in 5083 aluminum, 300X.



Figure 44. Fatigue striae in 5083 aluminum, 1000X.

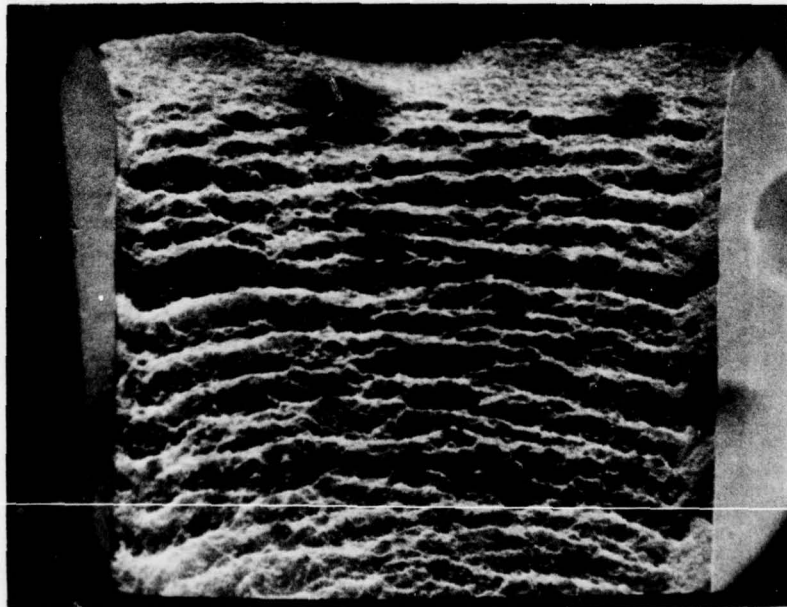


Figure 45. 5083 aluminum Charpy impact specimen tested at -196°C , 10X.

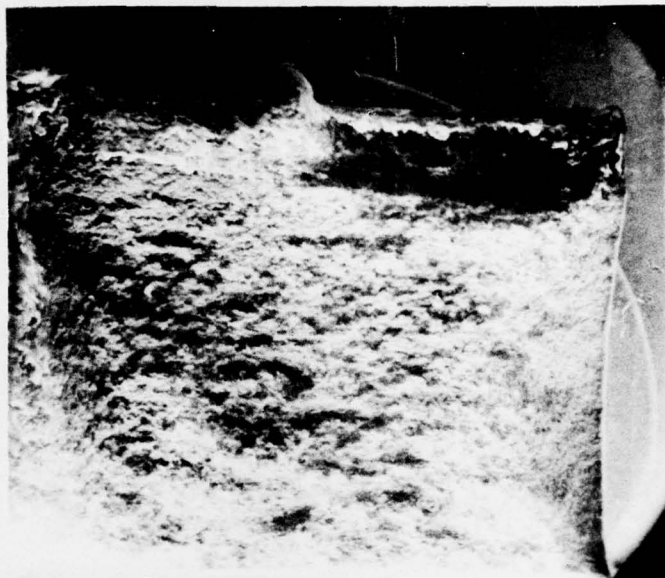


Figure 46. 5083 aluminum Charpy impact specimen tested at 0°C, 11X.

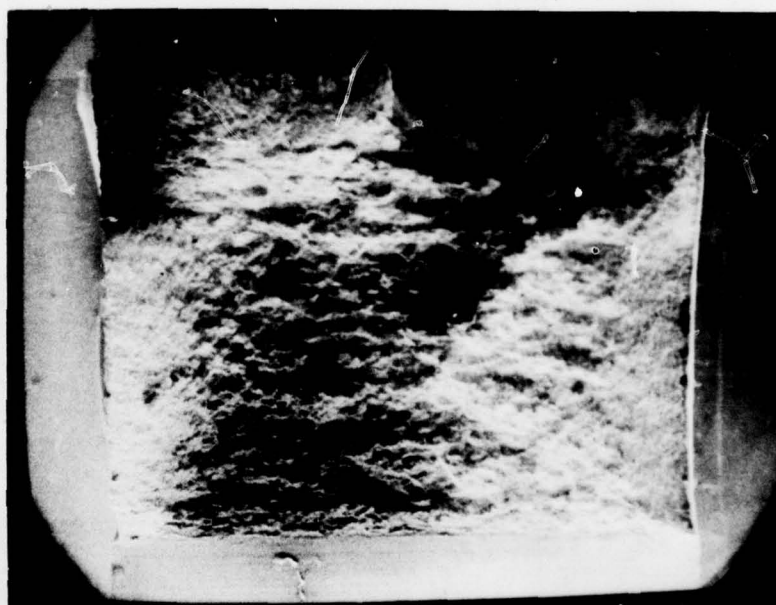


Figure 47. 5083 aluminum Charpy impact specimen tested at 25°C, 11X.

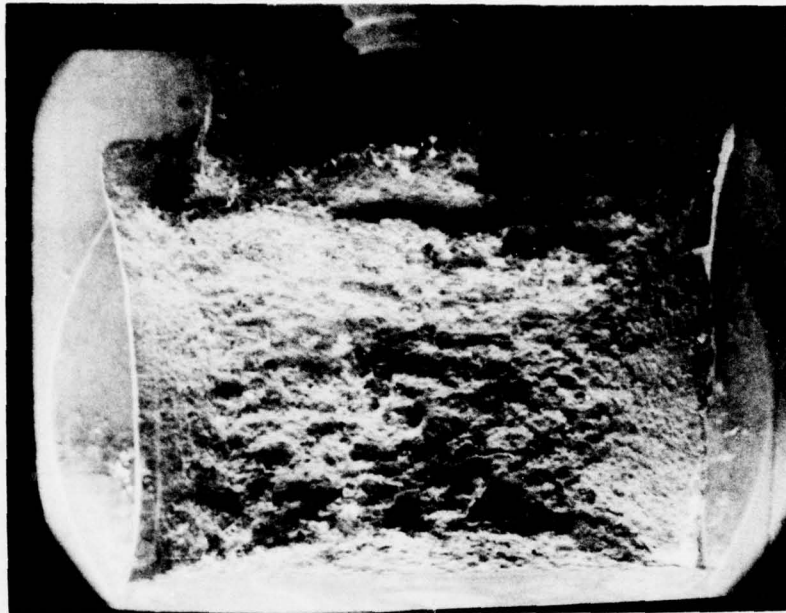


Figure 48. 5083 aluminum Charpy impact specimen tested at 100°C, 11X.

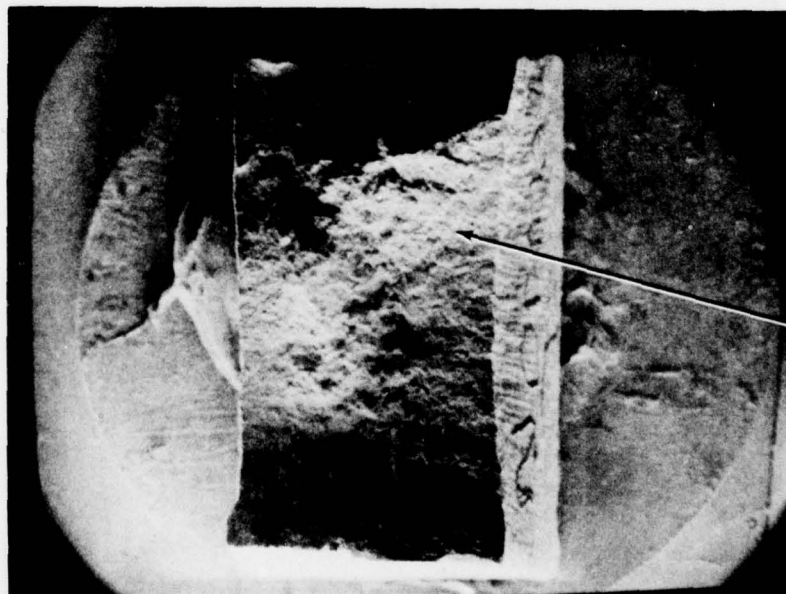


Figure 50

Figure 49. Tensile fracture surface of 6061 aluminum, 10X.

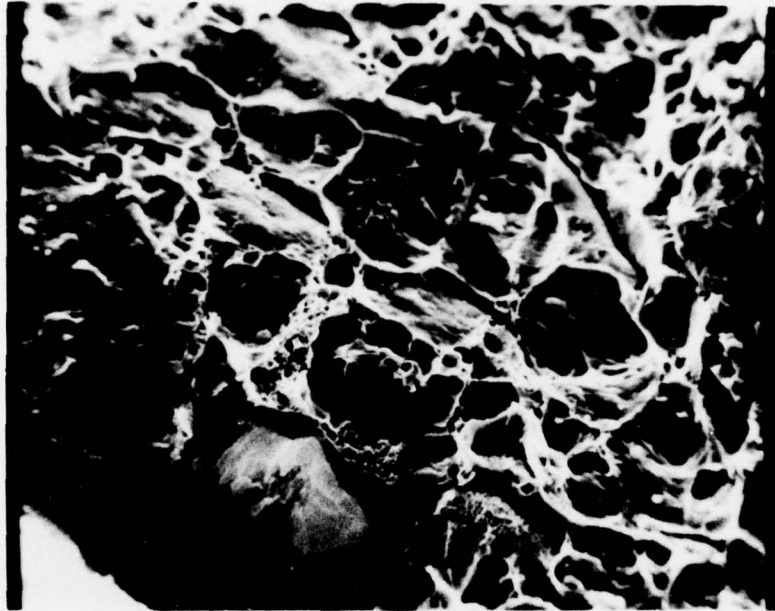


Figure 50. Dimple rupture in 6061 aluminum fracture surface, 300X.

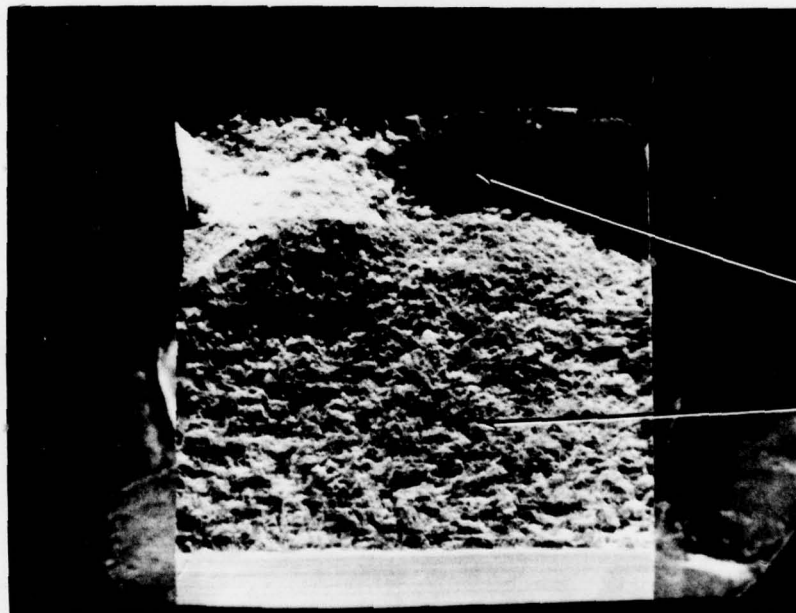
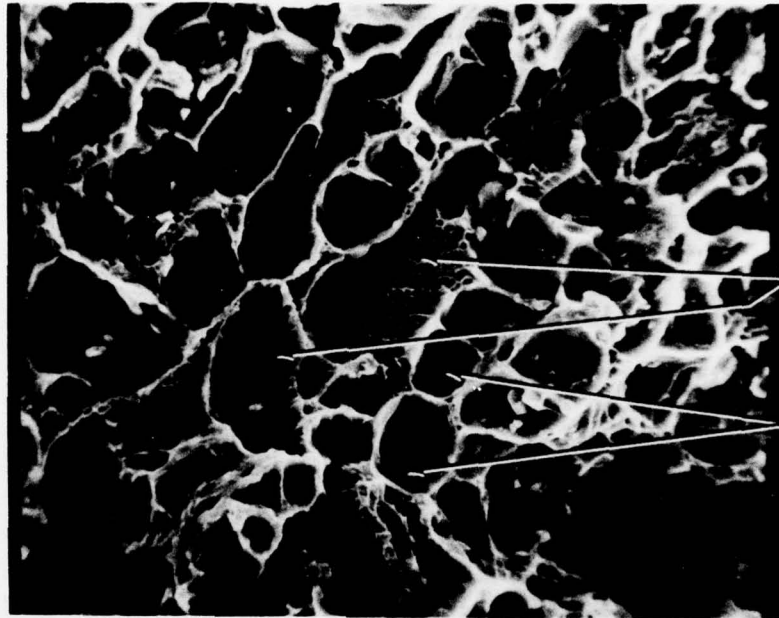


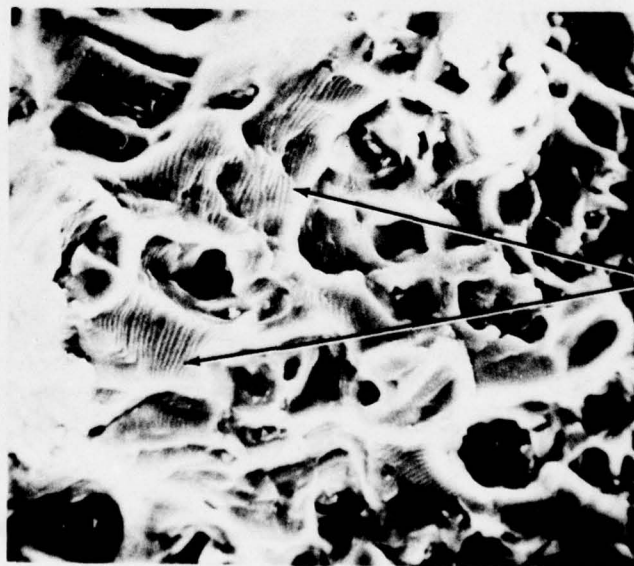
Figure 51. Fatigue fracture surface of 6061 aluminum, 13X.



Fine-Grained
Dimple Structure

Coarse Dimple
Structure

Figure 52. Dimple rupture in 6061 aluminum fatigue fracture surface, 300X.



Fatigue Striae

Figure 53. Fatigue striae in 6061 aluminum, 300X.

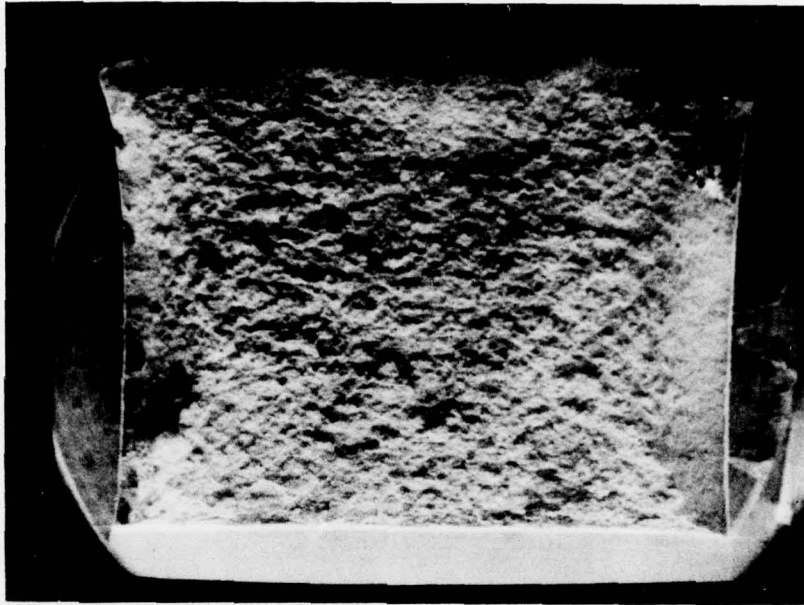


Figure 54. 6061 aluminum Charpy impact specimen tested at -196°C , 11X.

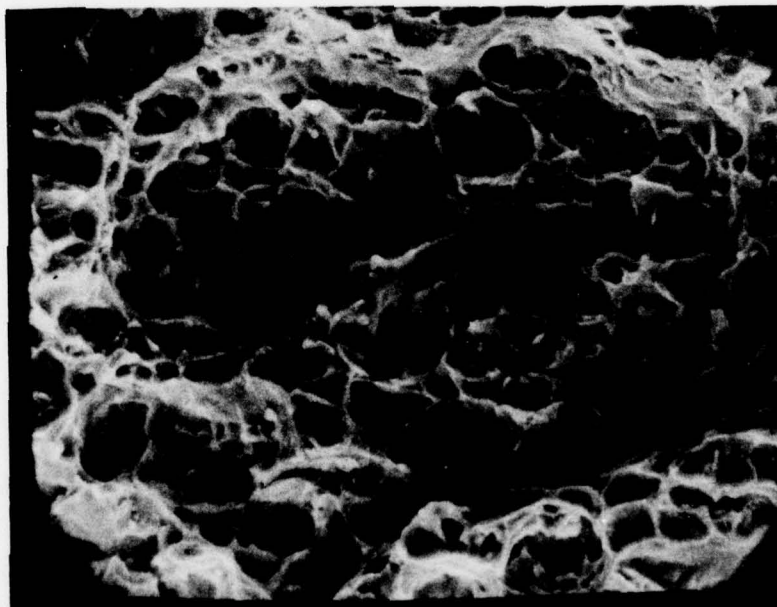


Figure 55. Dimple rupture in 6061 aluminum Charpy impact specimen tested at -196°C , 550X.

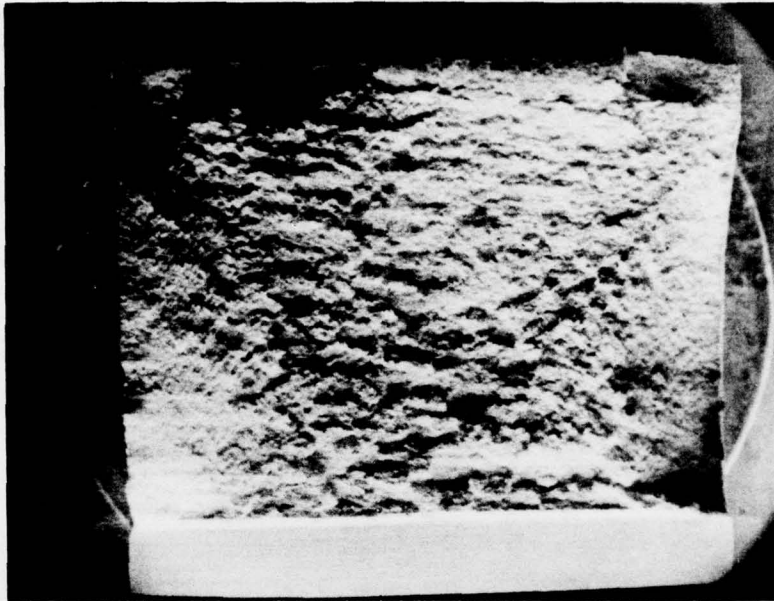


Figure 56. 6061 aluminum Charpy impact specimen tested at 0°C, 10X.

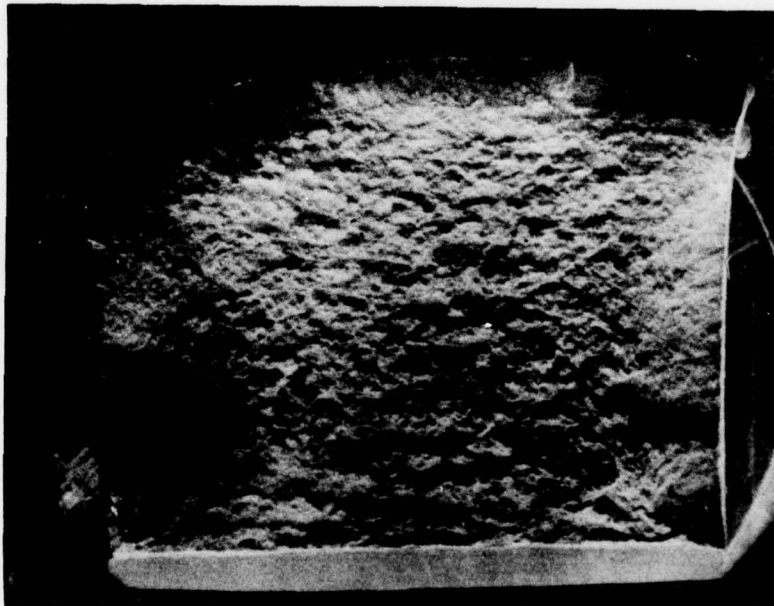


Figure 57. 6061 aluminum Charpy impact specimen tested at 25°C, 11X.

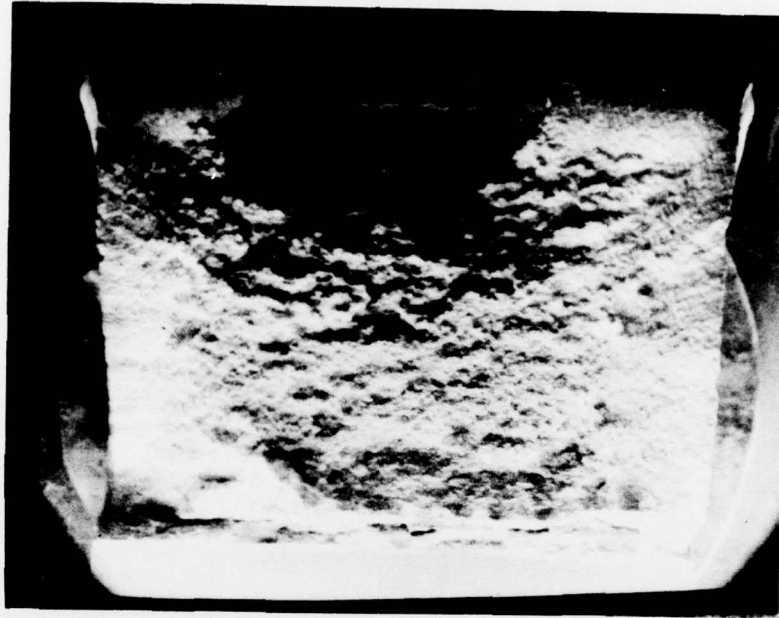


Figure 58. 6061 aluminum Charpy impact specimen tested at 100°C, 11X.